



NUREG/CR-5049  
ORNL/TM-10651

**OAK RIDGE  
NATIONAL  
LABORATORY**

**MARTIN MARIETTA**

**Pressure Vessel Fluence  
Analysis and Neutron Dosimetry**

F. B. K. Kam  
R. E. Maerker  
M. L. Williams  
F. W. Stallmann

Prepared for the  
U.S. Nuclear Regulatory Commission  
Office of Nuclear Regulatory Research  
under Interagency Agreement DOE 0551-0551-A1

OPERATED BY  
MARTIN MARIETTA ENERGY SYSTEMS, INC.  
FOR THE UNITED STATES  
DEPARTMENT OF ENERGY

8802240213 871231  
PDR NUREG  
CR-5049 R PDR

#### NOTICE

This report was prepared as an account of work sponsored by an agency of the United States Government. Neither the United States Government nor any agency thereof, or any of their employees, makes any warranty, expressed or implied, or assumes any legal liability or responsibility for any third party's use, or the results of such use, of any information, apparatus product or process disclosed in this report, or represents that its use by such third party would not infringe privately owned rights.

Available from

Superintendent of Documents  
U.S. Government Printing Office  
Post Office Box 37082  
Washington, D.C. 20013-7982

and

National Technical Information Service  
Springfield, VA 22161

Research Reactors Division

PRESSURE VESSEL FLUENCE ANALYSIS AND NEUTRON DOSIMETRY

F. B. K. Kam  
R. E. Maerker  
M. L. Williams  
F. W. Stallmann

Manuscript Completed - November 1987  
Date Published - December 1987

NOTICE: This document contains information of a preliminary nature. It is subject to revision or correction and therefore does not represent a final report.

Prepared for the  
U.S. Nuclear Regulatory Commission  
Office of Nuclear Regulatory Research  
Washington, D.C. 20555  
under Interagency Agreement DOE 0551-0551-A1

NRC FIN B0415

Prepared by the  
Oak Ridge National Laboratory  
Oak Ridge, Tennessee 37831  
operated by  
MARTIN MARIETTA ENERGY SYSTEMS, INC.  
for the  
U.S. DEPARTMENT OF ENERGY  
under contract DE-AC05-84OR21400

## TABLE OF CONTENTS

	<u>Page</u>
FIGURE LIST . . . . .	v
TABLE LIST . . . . .	vii
ABSTRACT . . . . .	ix
1. INTRODUCTION . . . . .	1
2. CURRENT METHODOLOGY . . . . .	3
2.1 OVERVIEW . . . . .	3
2.2 EQUATIONS AND DEFINITIONS . . . . .	4
2.3 SAMPLE DISCRETE ORDINATES TRANSPORT CALCULATIONS . . . . .	8
2.4 NEUTRON DOSIMETRY FOR SAMPLE RPV ANALYSIS . . . . .	19
2.5 RESULT OF SAMPLE RPV ANALYSIS . . . . .	21
3. SHORTCOMINGS IN THE PRESENT RPV ANALYSIS PROCEDURE . . . . .	25
3.1 CROSS-SECTION SET STANDARDIZATION . . . . .	25
3.2 ABSOLUTE COMPARISONS BETWEEN CALCULATED AND MEASURED DOSIMETER ACTIVITIES . . . . .	25
3.3 APPROXIMATIONS IN THE TRANSPORT CALCULATIONS . . . . .	26
3.4 MULTI-CYCLE ANALYSIS . . . . .	27
3.5 CONSOLIDATION OF MEASURED AND CALCULATED RESULTS . . . . .	27
4. RECOMMENDED IMPROVEMENTS IN RPV TRANSPORT ANALYSIS PROCEDURES . . . . .	29
4.1 OVERVIEW . . . . .	29
4.2 STANDARDIZED NUCLEAR DATA . . . . .	29
4.3 STANDARDIZED DISCRETE ORDINATES METHODOLOGY . . . . .	30
4.4 TREATMENT OF SPACE- AND TIME-DEPENDENT EFFECTS . . . . .	31
4.4.1 Space-Dependent Source Distribution . . . . .	32
4.4.2 Time-Dependent Variations in the Source Over a Cycle . . . . .	33
4.4.3 Cycle-Dependent Source Variations . . . . .	40
4.4.4 Three-Dimensional Flux Synthesis . . . . .	41

TABLE OF CONTENTS  
(continued)

	<u>Page</u>
4.5 CONSOLIDATION OF TRANSPORT CALCULATION AND DOSIMETRY MEASUREMENTS . . . . .	44
4.5.1 Adjoint Version of the Conventional Method . . . . .	45
4.5.2 Least-Squares Consolidation . . . . .	47
5. CONCLUSIONS AND RECOMMENDATIONS . . . . .	51
6. REFERENCES . . . . .	53

## FIGURE LIST

	<u>Page</u>
2.1. R- $\theta$ reactor geometry . . . . .	12
2.2. Plan view of a reactor vessel surveillance capsule . . . . .	13
2.3. Calculated radial distribution of maximum neutron fluence rates ( $E > 1.0$ MeV) within the pressure vessel . . . . .	13
2.4. Calculated radial distribution of maximum fast neutron flux ( $E > 1.0$ MeV) within the pressure vessel . . . . .	14
2.5. Relative axial variation of fast neutron flux ( $E > 1.0$ MeV) within the pressure vessel . . . . .	15
2.6. Calculated radial distribution of maximum fast neutron flux ( $E > 1.0$ MeV) within the surveillance capsule . . . . .	16
2.7. Calculated variation of fast neutron flux monitor saturated activity within capsule located at $40^\circ$ . . . . .	17
2.8. Calculated variation of fast neutron flux monitor saturated activity within capsule located at $4^\circ$ . . . . .	18

TABLE LIST

	<u>Page</u>
2.1. 47-group energy structure of SAILOR cross-section library . . . . .	9
2.2. Calculated neutron energy spectra at the center of the surveillance capsules . . . . .	10
2.3. Calculated fast neutron flux ( $E > 1.0$ MeV) and lead factors for surveillance capsules . . . . .	11
2.4. Spectrum-averaged reaction cross sections at the center of surveillance capsules . . . . .	11
2.5. Nuclear parameters for neutron flux monitors . . . . .	20
2.6. Irradiation history of surveillance capsule . . . . .	20
2.7. Results of thermal neutron dosimetry for surveillance capsule . . . . .	21
2.8. Measured saturated activities and derived fluence and fluence rates for surveillance capsule . . . . .	23
2.9. Comparison of measurements and calculations for surveillance capsule . . . . .	24
2.10. Summary of neutron dosimetry results . . . . .	24

## ABSTRACT

A review of the various methodologies used by industries and research institutes for reactor pressure vessel (RPV) fluence determination shows that most organizations employ an analysis sequence consisting of three steps. These include transport calculations, dosimetry measurements, and a statistical procedure to combine the calculations and measurements to arrive at a fluence value which has a smaller uncertainty than the original calculations. An accurate determination of damage fluence accumulated by the RPV as a function of space and time is essential in order to ensure the vessel integrity for both pressurized thermal shock transients and end-of-life considerations. The desired accuracy for neutron exposure parameters such as displacements per atom or neutron fluence ( $E > 1.0$  MeV) is of the order of  $\pm 10\%$  to  $\pm 15\%$  (10).<sup>\*</sup> These types of accuracies can only be obtained realistically by validation of the entire analysis sequence in benchmark experiments. This report identifies a standardized procedure based on benchmarked calculations, data, and dosimetry measurements, which could be used by organizations performing RPV fluence determinations. Another purpose of this report is to provide supporting documentation for any proposed regulatory guide on this subject.

---

<sup>\*</sup>ASTM Standard E706-84, "Master Matrix for Light Water Reactor Pressure Vessel Surveillance Standards," 1987 Annual Book of Standards, Section 12, Volume 12.02, American Society for Testing and Materials, Philadelphia, PA, 1987.

## 1. INTRODUCTION

Pressure vessel surveillance capsules historically have been incorporated into the design of power reactors because of the need to continuously monitor the accumulation of neutron fluence at critical pressure vessel locations during reactor operation.<sup>1-4</sup> The capsules, usually placed in the downcomer region, contain both metallurgical specimens of correlated material used in the weldments and plate of the reactor pressure vessel (RPV) as well as dosimetry foils. Analysis of the sequential extraction of these surveillance capsules necessitates the use of two dissimilar technical disciplines. First, the measured foil activities are combined with the results of a neutron transport calculation to infer fluence rates at both the dosimeter location and at the critical pressure vessel locations. Projected fluences based on this analysis provide a progressively updated estimate for the remaining reactor operation time until some specified limiting criterion (e.g.,  $\Delta RT_{NDT}$  at the critical RPV locations) is reached. Second, analysis using fracture mechanics techniques of the specimens and/or use of specifications in Regulatory Guide 1.99<sup>5</sup> allows direct estimates to be made of the state of radiation damage to the RPV-type material. Since the capsule is usually located at a position of higher fluence than that in the pressure vessel, the metallurgical specimen damage is accelerated relative to that in the pressure vessel, and there thus exists a safety factor ("lead factor") inherent in the surveillance method.

There are two types of RPV critical locations in which radiation-weakened fracture toughness is a concern. The first type is located near the region of maximum fluence at a depth into the RPV of approximately one-quarter (1/4-T) the pressure vessel thickness, and its accumulated fluence generally determines the "nominal lifetime" of the RPV. The second type appears only in certain Pressurized Water Reactors (PWRs) and are located near the inner surface of the pressure vessel (0-T) at a longitudinal or circumferential weld containing appreciable copper or nickel, near the azimuth of maximum fluence. At these locations, the RPV nominal lifetime may be severely shortened by further limitations placed on the maximum allowable nil-ductility transition temperature placed on these welds, which generally increases with accumulated fluence. The nominal end-of-life determining locations are situated in the vicinity of the reactor midplane, whereas the locations sensitive to pressurized thermal shock (PTS) phenomena may be situated at considerable distances above or below the midplane.

This report discusses a three-step pressure vessel fluence determination analysis procedure which addresses:

1. transport calculations to compute the fluence spectra at surveillance locations and at critical locations throughout the RPV,
2. dosimetry measurements to determine reaction rates at surveillance locations and/or ex-vessel cavity locations, and
3. consolidation of measurements and calculations to reduce uncertainties of the neutron exposure parameters at the critical locations.

Its purpose is to review in detail the current methodology used for RPV fluence calculations and to describe recently developed techniques which could improve upon the accuracy of the present method in some instances, especially for extended lifetime operation in which cavity dosimetry will play a major role. There are currently no standardized procedures which must be followed by organizations performing RPV fluence calculations and, hence, the Nuclear Regulatory Commission (NRC) must assess the quality of the different analyses each time a surveillance capsule is analyzed. Variations in techniques and rigor can lead to variations in the accuracy of the estimated RPV fluence obtained by different organizations. Another purpose of the paper is to identify standardized, benchmarked methods and data which could be used by all organizations performing RPV transport calculations. In this way, quality assurance can be established. The report summarizes the present methodology of transport calculations in Section 2, and discusses its limitations in Section 3. Potential improvements and extensions in the methods for performing RPV calculations are described in Section 4. Conclusions and recommendations are presented in Section 5.

## 2. CURRENT METHODOLOGY

### 2.1 OVERVIEW

A more or less consensus methodology evolved during the late 1970s and early 1980s for performing RPV fluence calculations in the U.S. Although different organizations may employ variations, the general approach is similar and will be called the "current methodology" in this report. This methodology has been applied to the analysis of many different power reactors and has, in fact, been quite successful, when used in conjunction with in-vessel surveillance dosimetry, in providing reliable estimates for RPV fluence in currently operating plants. In this section, the current methodology which forms the basis for RPV fluence analysis in the U.S. today is reviewed and a sample application of the techniques is presented.

The current methodology for RPV fluence determination is based on combining results of transport calculations with measured dosimeter activities, usually taken from the surveillance capsules located inside of the pressure vessel. The transport calculations provide two crucial sets of data in the overall analysis: (1) spectrum-weighted, effective dosimeter cross sections and (2) lead factors for various points in the RPV.

The calculated one-group effective cross sections [see Eq. (2.2) for precise definition] for different dosimeters are divided into the respective measured reaction rates (obtained from saturated activities) in order to obtain the one-group flux greater than 1 MeV at the capsule location. The corresponding flux at various depths into the RPV is then obtained by dividing the capsule flux by the appropriate lead factors.

Note that both the effective cross sections and lead factors depend only on ratios of computed results so that absolute calculations are not required - the measured dosimeter activities provide the appropriate flux normalization. The insensitivity of the final results to the absolute calculated activities is both an advantage and disadvantage. The advantage is that results are less sensitive to calculational approximations. The disadvantages are that inconsistencies and uncertainties in the calculations are sometimes not apparent if the absolute agreement between computed and measured results is not examined, and that the experimental dosimeter measurements exclusively provide the normalization of the fluence estimate.

In Section 2.2, the mathematical expressions used in the current methodologies for RPV fluence determination are presented. In the following three sections, an actual RPV analysis study based on this methodology for a sample U.S. reactor is described.

## 2.2 EQUATIONS AND DEFINITIONS

In this section, the expressions used in the current methodology for RPV fluence determination are presented. The activity at time-of-removal (TOR) is defined to be the activity in some dosimeter "m" when it is removed from the reactor. This activity is presently computed from the approximate expression:

$$A_{\text{TOR}}^m = N_0^m Y \int_0^{\infty} \sigma^m(E) \phi(E) dE \sum_{j=1}^J P_j (1 - e^{-\lambda_m T_j}) e^{-\lambda_m (T - t_j)} \quad , \quad (2.1)$$

where  $A_{\text{TOR}}^m$  = product nuclide activity (Bq) in dosimeter "m" at time of removal (TOR),

$\sigma^m(E)$  = energy-dependent activation cross section ( $\text{cm}^2$ ) for dosimeter m,

$\phi(E)$  = energy-dependent fluence rate [ $\text{n}/(\text{cm}^2 \cdot \text{s} \cdot \text{eV})$ ] at surveillance location, calculated for full power using some representative, time-independent core source distribution that is typical of the fuel loading,

$Y$  = product nuclide per reaction (fission yield),

$\lambda_m$  = decay constant of the product nuclide ( $\text{d}^{-1}$ ) in dosimeter m,

$P_j$  = fraction of full power during operating period j,

$T_j$  = length of time (d) for irradiation interval j,

$T$  = time (d) from beginning of irradiation to time of removal,

$t_j$  = elapsed time (d) from beginning of irradiation to end of interval j,

$N_0^m$  = number of target atoms in dosimeter, and

$J$  = number of irradiation intervals.

Also the effective one-group cross section for dosimeter m is defined relative to an energy threshold  $E_t$ :

$$\bar{\sigma}_{E_t}^m = \frac{\int_0^{\infty} \sigma^m(E) \phi(E) dE}{\int_{E_t}^{\infty} \phi(E) dE} \quad , \quad (2.2)$$

where  $\bar{\sigma}_{E_t}^m$  = effective spectrum-averaged cross section,

$$\int_{E_t}^{\infty} \phi(E) dE = \text{fluence rate for neutrons with energies greater than } E_t, [\phi(E > E_t)], \text{ and}$$

$$\int_0^{\infty} \sigma^m(E) \phi(E) dE = \text{reaction rate (per atom) of dosimeter nuclide } m, (\text{ASAT}).$$

From Eq. (2.2), the saturated activity is defined by

$$A_{\text{SAT}}^m = \phi(E > E_t) \cdot \bar{\sigma}_{E_t}^m = \text{dosimeter reaction rate per atom} \quad (2.3) \\ \text{Bq/atom, or reactions/s per atom.}$$

Substituting Eq. (2.3) into Eq. (2.1) and solving for ASAT and  $\phi(E > E_t)$ , one obtains,

$$A_{\text{SAT}}^m = \frac{A_{\text{TOR}}^m}{N_0^m Y \sum_{j=1}^J P_j (1 - e^{-\lambda_m T_j}) e^{-\lambda_m (T - t_j)}} \quad (2.4)$$

and

$$\phi(E > E_t) = \frac{A_{\text{TOR}}^m}{N_0^m Y \bar{\sigma}_{E_t}^m \sum_{j=1}^J P_j (1 - e^{-\lambda_m T_j}) e^{-\lambda_m (T - t_j)}}$$

Defining the "saturation factor" (SF) to be

$$\text{SF} = \frac{1}{\sum_{j=1}^J P_j (1 - e^{-\lambda_m T_j}) e^{-\lambda_m (T - t_j)}}$$

one has, therefore,

$$\phi(E > E_t) = \frac{A_{\text{TOR}}^m \cdot \text{SF}}{N_0^m Y \bar{\sigma}_{E_t}^m} = \frac{A_{\text{SAT}}^m}{\bar{\sigma}_{E_t}^m} \quad (2.5)$$

From Eq. (2.5), it can be seen that the value for  $\phi(E > E_t)$  can be obtained by dividing the saturated activity by the effective cross section. In practice, ASAT is obtained from the dosimeter measurements while  $\bar{\sigma}_{E_t}^m$  is obtained from the transport calculations. Using this approach and defining the calculated saturated activity to be

$$(A_{\text{SAT}}^m)_{\text{calc}} = \int_0^{\infty} \bar{\sigma}^m(E) \phi_{\text{calc}}(E) dE \quad ,$$

the effective cross section in Eq. (2.2) can be expressed as

$$\bar{\sigma}_{E_t}^m = \frac{(ASAT)_{calc}^m}{\phi_{calc}^{sc}(E>E_t)}$$

where  $\phi_{calc}^{sc}(E>E_t)$  is the value of the threshold flux in the surveillance capsule obtained from the transport calculation.

Substituting the above relation into Eq. (2.5) gives the "adjusted" capsule flux

$$\phi_{adj}^{sc}(E>E_t) = \frac{(ASAT)_{meas}^m}{(ASAT)_{calc}^m} \cdot \phi_{calc}^{sc}(E>E_t) \quad (2.5a)$$

Thus, it can be seen that the present methodology is equivalent to simply scaling the calculated, integrated-flux by the ratio of the measured-to-computed saturated activities. In reality, this ratio varies somewhat for the different dosimeters, so that the average value of the ratio should be used. The following notation will be used for this average ratio:

$$\left\langle \frac{(ASAT)_{meas}^m}{(ASAT)_{calc}^m} \right\rangle = \frac{1}{M} \sum_{m=1}^M \frac{(ASAT)_{meas}^m}{(ASAT)_{calc}^m}$$

The thermal neutron fluence rate ( $\phi_{th}$ ) used to correct for dosimeter burnout is determined from the bare and cadmium-covered cobalt activities using Eq. (2.6) below:

$$\phi_{th} = \frac{A_B - A_{Cd}}{N_0 \sigma_0 \sum_{j=1}^J P_j (1 - e^{-\lambda T_j}) e^{-\lambda(T-t_j)}} \quad (2.6)$$

where  $A_B$  = bare cobalt activity (dps/mg),

$A_{Cd}$  = cadmium-covered cobalt activity (dps/mg),

$N_0$  = number of cobalt-59 atoms per mg of cobalt,

$\sigma_0$  = 37.1 barns, and

$\lambda$  = 0.0003601 d<sup>-1</sup>.

The lead factor (LF) is defined as follows

$$LF \stackrel{d}{=} \frac{\text{neutron fluence rate } (E>E_t) \text{ calculated at capsule center}}{\text{maximum neutron-fluence rate calculated at PV inner radius}} \quad (2.7)$$

$$= \frac{\phi_{calc}^{sc}(E>E_t)}{\phi_{calc}^{IR}(E>E_t)}$$

A generalization of this lead factor definition may be readily extended to any location of interest in the pressure vessel by replacing the denominator in Eq. (2.8) by the neutron fluence rate at that particular location  $\ell$ :

$$LF_{\ell} = \frac{\phi_{\text{calc}}^{\text{sc}}(E>E_t)}{\phi_{\text{calc}}^{\ell}(E>E_t)} \quad . \quad (2.8)$$

This parameter is computed based on the results of the transport calculations and is used to propagate the fluence at the capsule into the RPV.

The final threshold flux incident on the RPV is determined using the expression:

$$\phi^{\text{IR}}(E>E_t) = \frac{\phi_{\text{adj}}^{\text{sc}}(E>E_t)}{LF} \quad , \quad (2.9)$$

where  $\phi_{\text{adj}}^{\text{sc}}$  is the adjusted capsule flux from Eq. (2.5a) and LF is the lead factor from Eq. (2.7). Using these expressions in Eq. (2.9) gives

$$\begin{aligned} \phi^{\text{IR}}(E>E_t) &= \left[ \left\langle \frac{(A_{\text{SAT}})_{\text{meas}}}{(A_{\text{SAT}})_{\text{calc}}} \right\rangle \phi_{\text{adj}}^{\text{sc}}(E>E_t) \right] \left[ \frac{\phi_{\text{calc}}^{\text{IR}}(E>E_t)}{\phi_{\text{calc}}^{\text{sc}}(E>E_t)} \right] \\ \phi^{\text{IR}}(E>E_t) &= \left\langle \frac{(A_{\text{SAT}})_{\text{meas}}}{(A_{\text{SAT}})_{\text{calc}}} \right\rangle \phi_{\text{calc}}^{\text{IR}}(E>E_t) \quad . \quad (2.10) \end{aligned}$$

Equation (2.10) shows that the final RPV threshold flux is obtained in the current methodology by "adjusting" the calculated RPV flux by the average ratio of the measured-to-calculated saturated activities at the surveillance location; i.e., by the inverse of the average C/E (calculation/experiment) value.

Equation (2.10) gives the fluence ratio incident on the vessel; the fluence rate at other locations is obtained analogously by using the generalized definitions of the lead factor shown in Eq. (2.8). The result will be the same expression as Eq. (2.10) with the calculated incident flux replaced by the calculated flux at the point of interest. In all cases, the "adjustment factor"  $(A_{\text{SAT}})_{\text{meas}}/(A_{\text{SAT}})_{\text{calc}}$  will be the same.

After determining the fluence rate from Eq. (2.10), the total fluence is obtained by:

$$\phi^{\text{IR}}(E>E_t) = \phi^{\text{IR}}(E>E_t) \sum_{j=1}^J P_j T_j \quad . \quad (2.11)$$

### 2.3 SAMPLE DISCRETE ORDINATES TRANSPORT CALCULATIONS

A typical transport calculation was performed by a U.S. service laboratory to obtain RPV fluences using the methodology described in the previous section. The radial and azimuthal fluence rate distributions were obtained from a 2-D R- $\theta$  discrete ordinates computation for the geometry shown in Figs. 2.1 and 2.2. A second transport calculation using an R-Z model of the reactor was done to obtain axial variations of the neutron fluence rate for the regions of interest. The inclusion of the surveillance capsules in the R- $\theta$  model is mandatory to account for the significant perturbation effect from the physical presence of the capsule. Both calculations were performed using the discrete ordinates code DOT<sup>6</sup> with the 47-group, SAILOR cross-section library. The energy structure is given in Table 2.1. An S<sub>8</sub> angular structure and a P<sub>3</sub> Legendre cross-section expansion were used in the computations.

The results of the transport calculations required for the RPV fluence analysis are presented in Figs. 2.3 through 2.8 and Tables 2.2 through 2.4.

The information presented in this section is typical of that presented to the NRC each time a surveillance capsule is analyzed at a nuclear power plant. This particular analysis was completed in 1983.

Table 2.1. 47-group energy structure of SAILOR cross-section library

Group	Lower energy (MeV)	Group	Lower energy (MeV)
1	14.19*	25	0.183
2	12.21	26	0.111
3	10.00	27	0.0674
4	8.61	28	0.0409
5	7.41	29	0.0318
6	6.07	30	0.0261
7	4.97	31	0.0242
8	3.68	32	0.0219
9	3.01	33	0.0150
10	2.73	34	$7.10 \times 10^{-3}$
11	2.47	35	$3.36 \times 10^{-3}$
12	2.37	36	$1.59 \times 10^{-3}$
13	2.35	37	$4.54 \times 10^{-4}$
14	2.23	38	$2.14 \times 10^{-4}$
15	1.92	39	$1.01 \times 10^{-4}$
16	1.65	40	$3.73 \times 10^{-5}$
17	1.35	41	$1.07 \times 10^{-5}$
18	1.00	42	$5.04 \times 10^{-6}$
19	0.821	43	$1.86 \times 10^{-6}$
20	0.743	44	$8.76 \times 10^{-7}$
21	0.608	45	$4.14 \times 10^{-7}$
22	0.498	46	$1.00 \times 10^{-7}$
23	0.369	47	0.00
24	0.298		

\*The upper energy of Group 1 is 17.33 MeV.

Table 2.2. Calculated neutron energy spectra at the center of the surveillance capsules

Group No.	$\phi$ [n/(cm <sup>2</sup> ·s)]		Group No.	$\phi$ [n/(cm <sup>2</sup> ·s)]	
	4° capsules	40° capsules		4° capsules	40° capsules
1	1.35 x 10 <sup>7</sup>	2.08 x 10 <sup>7</sup>	25	8.59 x 10 <sup>9</sup>	3.42 x 10 <sup>10</sup>
2	4.85 x 10 <sup>7</sup>	7.65 x 10 <sup>7</sup>	26	8.10 x 10 <sup>9</sup>	3.29 x 10 <sup>10</sup>
3	1.56 x 10 <sup>8</sup>	2.67 x 10 <sup>8</sup>	27	6.50 x 10 <sup>9</sup>	2.67 x 10 <sup>10</sup>
4	2.74 x 10 <sup>8</sup>	4.89 x 10 <sup>8</sup>	28	4.80 x 10 <sup>9</sup>	1.99 x 10 <sup>10</sup>
5	4.32 x 10 <sup>8</sup>	8.20 x 10 <sup>8</sup>	29	1.68 x 10 <sup>9</sup>	6.92 x 10 <sup>9</sup>
6	9.33 x 10 <sup>8</sup>	1.85 x 10 <sup>9</sup>	30	1.04 x 10 <sup>9</sup>	4.27 x 10 <sup>9</sup>
7	1.18 x 10 <sup>9</sup>	2.57 x 10 <sup>9</sup>	31	1.71 x 10 <sup>9</sup>	7.15 x 10 <sup>9</sup>
8	2.07 x 10 <sup>9</sup>	5.17 x 10 <sup>9</sup>	32	1.05 x 10 <sup>9</sup>	4.41 x 10 <sup>9</sup>
9	1.62 x 10 <sup>9</sup>	4.54 x 10 <sup>9</sup>	33	2.52 x 10 <sup>9</sup>	1.05 x 10 <sup>10</sup>
10	1.27 x 10 <sup>9</sup>	3.71 x 10 <sup>9</sup>	34	4.21 x 10 <sup>9</sup>	1.75 x 10 <sup>10</sup>
11	1.46 x 10 <sup>9</sup>	4.38 x 10 <sup>9</sup>	35	5.66 x 10 <sup>9</sup>	2.35 x 10 <sup>10</sup>
12	7.19 x 10 <sup>9</sup>	2.19 x 10 <sup>9</sup>	36	5.16 x 10 <sup>9</sup>	2.17 x 10 <sup>10</sup>
13	2.12 x 10 <sup>9</sup>	6.52 x 10 <sup>9</sup>	37	7.79 x 10 <sup>9</sup>	3.31 x 10 <sup>10</sup>
14	1.04 x 10 <sup>9</sup>	3.22 x 10 <sup>9</sup>	38	4.42 x 10 <sup>9</sup>	1.88 x 10 <sup>10</sup>
15	2.67 x 10 <sup>9</sup>	8.37 x 10 <sup>9</sup>	39	4.68 x 10 <sup>9</sup>	2.01 x 10 <sup>10</sup>
16	3.21 x 10 <sup>9</sup>	1.05 x 10 <sup>10</sup>	40	6.27 x 10 <sup>9</sup>	2.71 x 10 <sup>10</sup>
17	4.67 x 10 <sup>9</sup>	1.57 x 10 <sup>10</sup>	41	7.59 x 10 <sup>9</sup>	3.31 x 10 <sup>10</sup>
18	8.45 x 10 <sup>9</sup>	2.98 x 10 <sup>10</sup>	42	4.33 x 10 <sup>9</sup>	1.90 x 10 <sup>10</sup>
19	5.73 x 10 <sup>9</sup>	2.09 x 10 <sup>10</sup>	43	5.24 x 10 <sup>9</sup>	2.31 x 10 <sup>10</sup>
20	2.83 x 10 <sup>9</sup>	1.04 x 10 <sup>10</sup>	44	3.46 x 10 <sup>9</sup>	1.53 x 10 <sup>10</sup>
21	8.14 x 10 <sup>9</sup>	3.14 x 10 <sup>10</sup>	45	2.93 x 10 <sup>9</sup>	1.29 x 10 <sup>10</sup>
22	6.21 x 10 <sup>9</sup>	2.45 x 10 <sup>10</sup>	46	5.59 x 10 <sup>9</sup>	2.41 x 10 <sup>10</sup>
23	7.46 x 10 <sup>9</sup>	2.93 x 10 <sup>10</sup>	47	1.41 x 10 <sup>10</sup>	5.66 x 10 <sup>10</sup>
24	6.51 x 10 <sup>9</sup>	2.59 x 10 <sup>10</sup>			

Table 2.3. Calculated fast neutron flux ( $E > 1.0$  MeV) and lead factors for surveillance capsules

Capsule identification	$\phi(E > 1.0 \text{ MeV})$ [n/(cm <sup>2</sup> ·s)]	Lead factors for 4° capsules	Lead factors for 40° capsules
Capsules at 4° (S, V, W, and Z)	$3.04 \times 10^{10}$		
Capsules at 40° (T, U, X, and Y)	$9.44 \times 10^{10}$		
Vessel IR	$2.98 \times 10^{10}$	1.02	3.17
Vessel 1/4-T	$1.65 \times 10^{10}$	1.84	5.72
Vessel 3/4-T	$3.41 \times 10^9$	8.92	27.7

Table 2.4. Spectrum-averaged reaction cross sections<sup>a</sup> at the center of surveillance capsules

Reaction	$\bar{\sigma}$ (barns)	
	Capsules at 4°	Capsules at 40°
$^{54}\text{Fe}(n,p)^{54}\text{Mn}$	0.0980	0.0735
$^{63}\text{Cu}(n,\alpha)^{60}\text{Co}$	0.00112	0.000659
$^{58}\text{Ni}(n,p)^{58}\text{Co}$	0.127	0.0993
$^{237}\text{Np}(n,f)^{137}\text{Cs}$	2.62	2.83
$^{238}\text{U}(n,f)^{137}\text{Cs}$	0.385	0.385

$$^a \bar{\sigma} = \frac{\int_0^{\infty} \sigma(E) \phi(E) dE}{\int_{1 \text{ MeV}}^{\infty} \phi(E) dE}$$

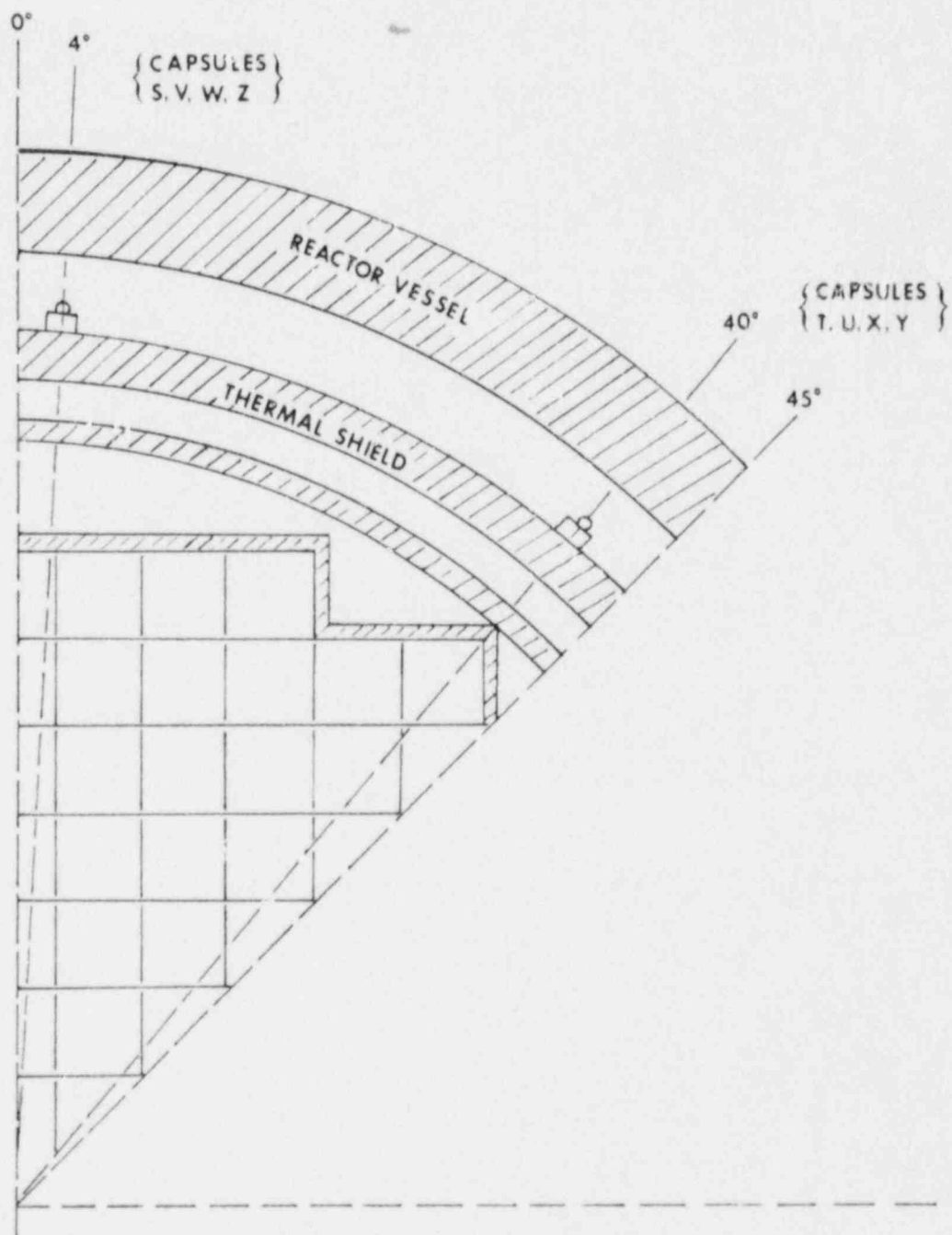


Fig. 2.1. Sequoyah Unit 2 R-θ reactor geometry.

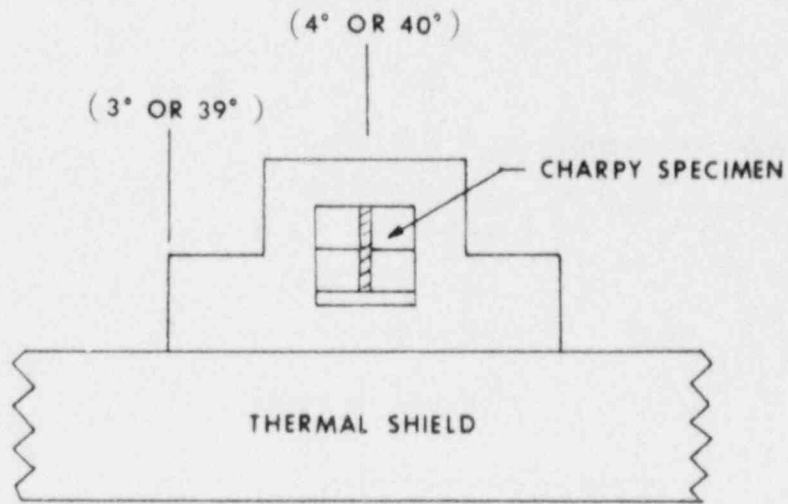


Fig. 2.2. Plan view of a reactor vessel surveillance capsule.

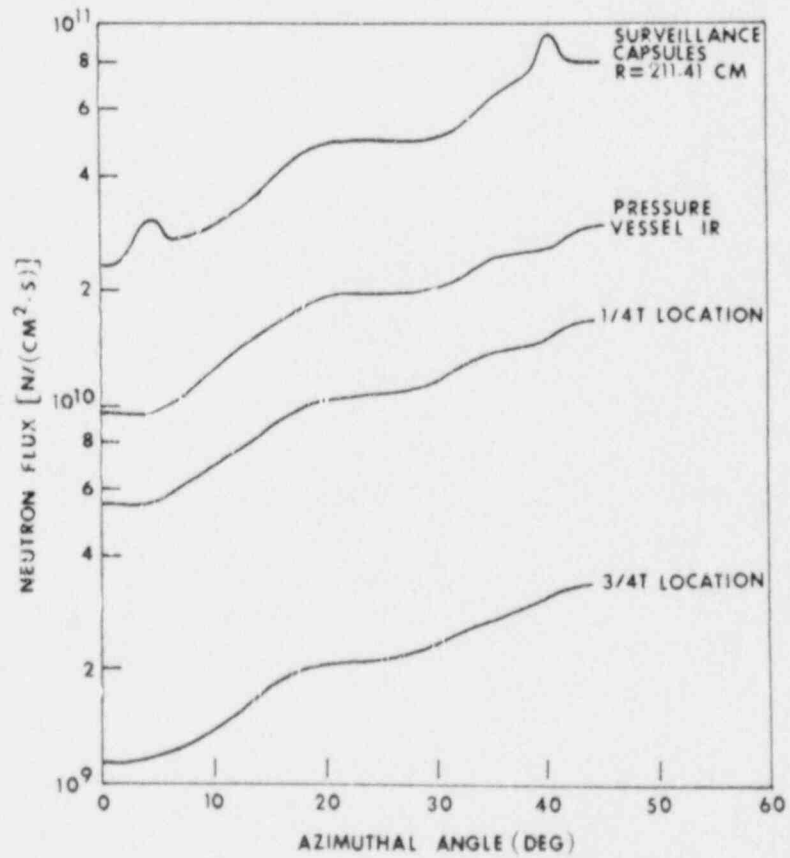


Fig. 2.3. Calculated radial distribution of maximum neutron fluence rates ( $E > 1.0$  MeV) within the pressure vessel.

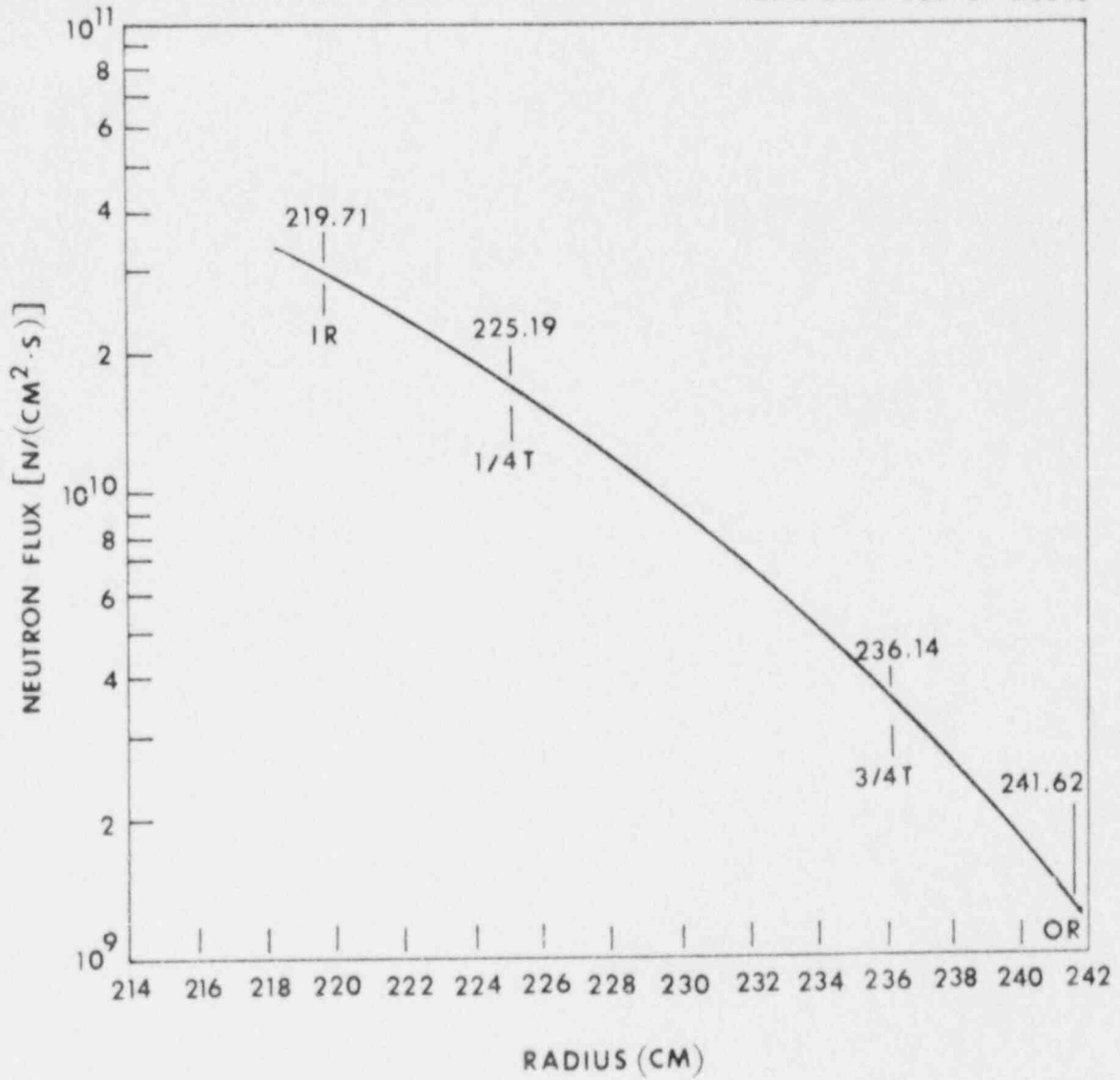


Fig. 2.4. Calculated radial distribution of maximum fast neutron flux ( $E > 1.0$  MeV) within the pressure vessel.

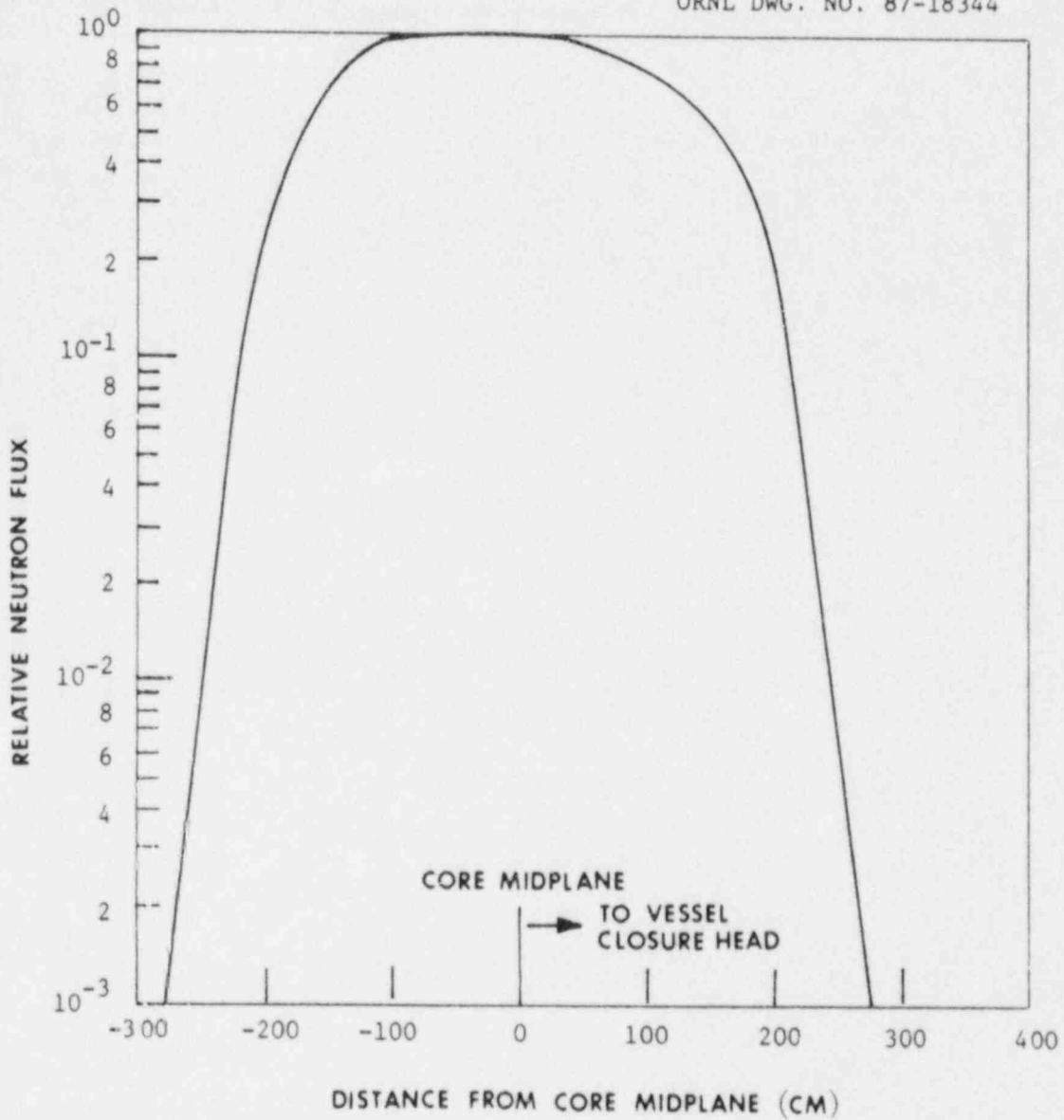


FIG. 2.5. Relative axial variation of fast neutron flux ( $E > 1.0$  MeV) within the pressure vessel.

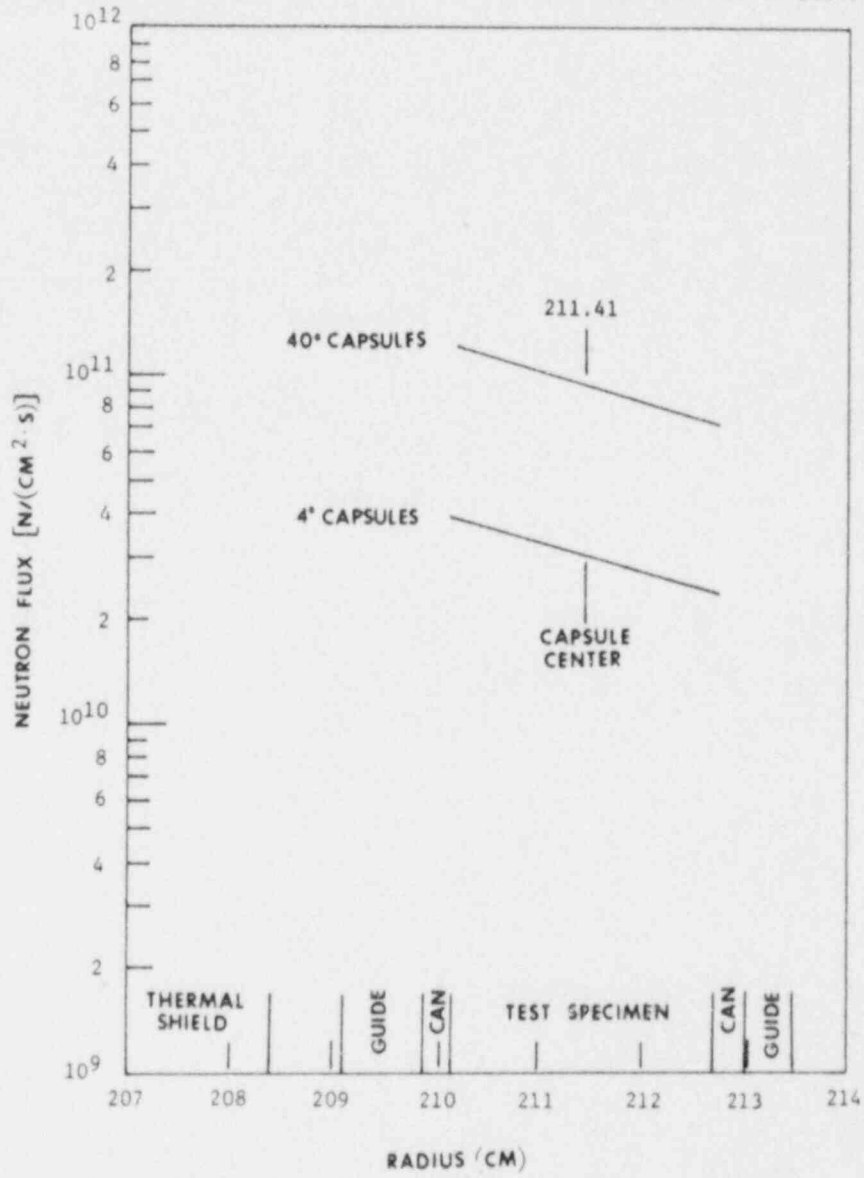


Fig. 2.6. Calculated radial distribution of maximum fast neutron flux ( $E > 1.0$  MeV) within the surveillance capsule.

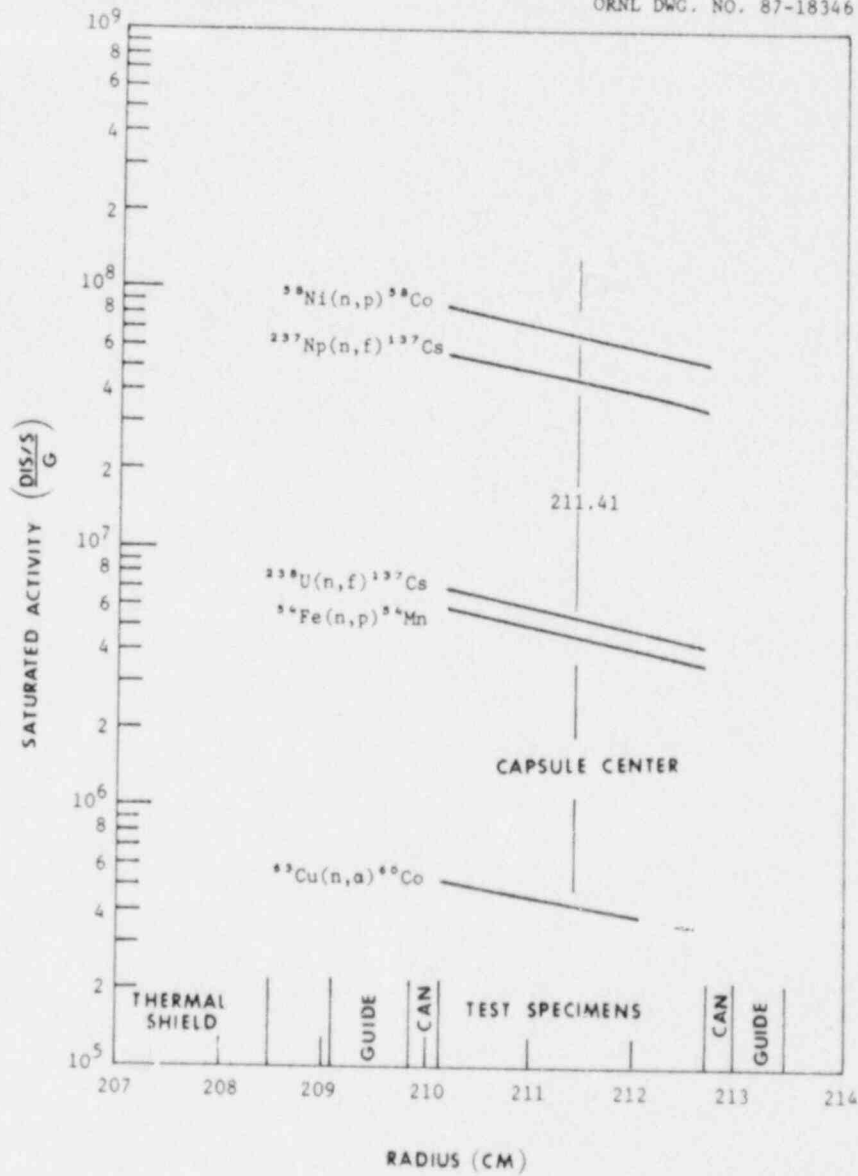


Fig. 2.7. Calculated variation of fast neutron flux monitor saturated activity within capsule located at 40°.

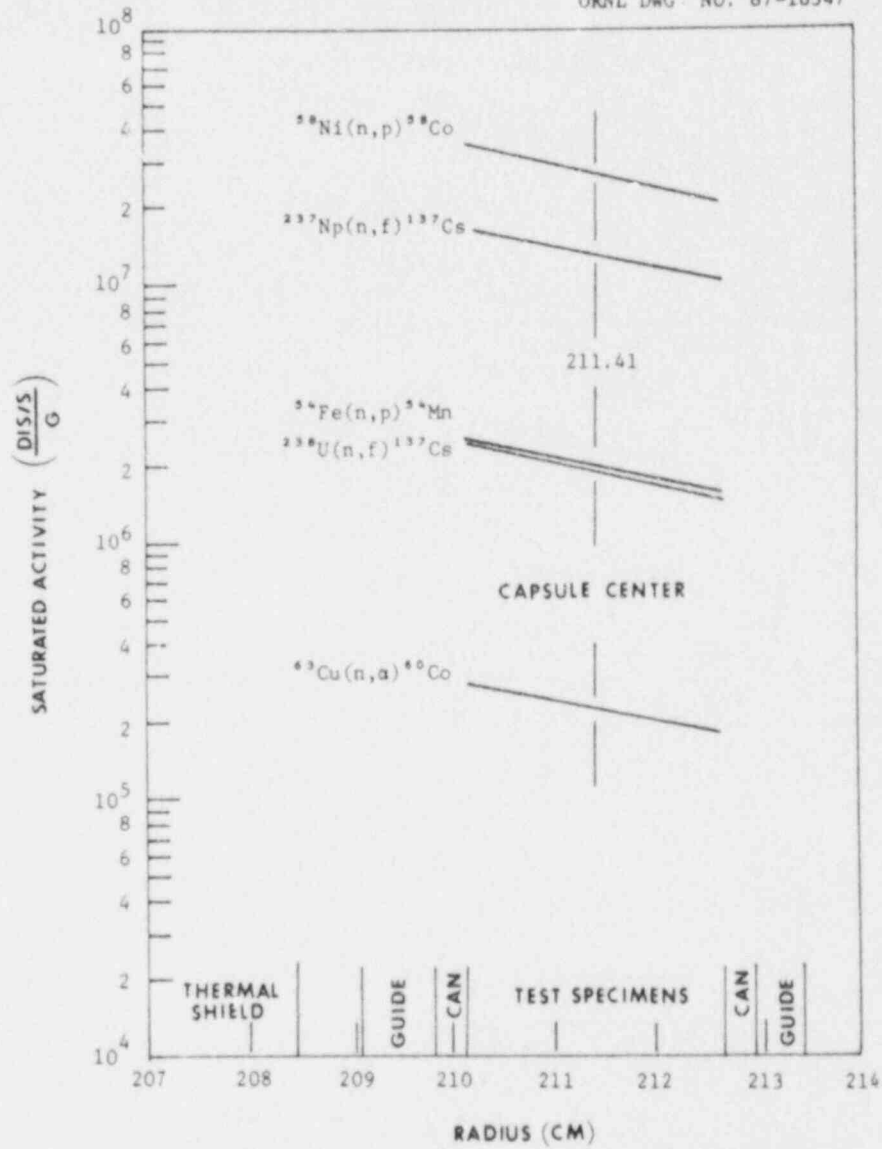


Fig. 2.8. Calculated variation of fast neutron flux monitor saturated activity within capsule located at  $4^\circ$ .

## 2.4 NEUTRON DOSIMETRY FOR SAMPLE RPV ANALYSIS

The neutron dosimeters and the constants used in processing the dosimeters for the sample reactor are given in Table 2.4, and the power-time history for the irradiation is given in Table 2.5.

The references for the procedures used in processing the dosimeters are

- ASTM E261-77, "Determining Neutron Flux, Fluence, and Spectra by Radioactivation Techniques"
- ASTM E262-77, "Determining Thermal Neutron Flux by Radioactive Techniques"
- ASTM E263-77, "Determining Fast Neutron Flux by Radioactivation of Iron"
- ASTM E264-77, "Determining Fast Neutron Flux by Radioactivation of Nickel"
- ASTM E523-76, "Measuring Fast Neutron Flux Density by Radioactivation of Copper"
- ASTM E704-79, "Determining Fast Neutron Flux Density by Radioactivation of Uranium-238"
- ASTM E705-79, "Determining Fast Neutron Flux Density by Radioactivation of Neptunium-237"

The thermal fluence rate,  $\phi_{th}$ , is determined from the measured bare and cadmium-covered cobalt activity using Eq. (2.6). This fluence rate (Table 2.7) is used to correct the fission and threshold activities from burnin and burnout.

The saturated activities ( $A_{SAT}$ ) in Table 2.8 are determined from the measured activities,  $A_{TOR}$ , using Eq. (2.4). If the radial gradients of the activities are significant in the capsule, the calculated gradients shown in Fig. 2.7 or Fig. 2.8 are used to adjust the saturated activities to a common location, the capsule center (Table 2.8). The measured dosimetry results and the derived fluence rates and fluences in the center of the capsule are given in Table 2.8 using Eqs. (2.5) and (2.6), respectively. Axial and azimuthal gradients may also be corrected using the results of the transport calculations discussed in Section 2.3. Finally, a comparison of measurements and calculations is presented in Table 2.9 to provide some measure of the discrepancies in the calculations.

Table 2.5. Nuclear parameters for neutron flux monitors

Monitor material	Reaction of interest	Target weight fraction	Response range	Product half-life	Fission yield (%)
Copper	$^{63}\text{Cu}(n,\alpha)^{60}\text{Co}$	0.6917	$E > 4.7 \text{ MeV}$	5.27 years	
Iron	$^{54}\text{Fe}(n,p)^{54}\text{Mn}$	0.0585	$E > 1.0 \text{ MeV}$	314 days	
Nickel	$^{58}\text{Ni}(n,p)^{58}\text{Co}$	0.6777	$E > 1.0 \text{ MeV}$	71.4 days	
U-238	$^{238}\text{U}(n,f)^{137}\text{Cs}$	1.0	$E > 0.4 \text{ MeV}$	30.2 years	6.3
Np-237	$^{237}\text{Np}(n,f)^{137}\text{Cs}$	1.0	$E > 0.08 \text{ MeV}$	30.2 years	6.5
Co-Al*	$^{59}\text{Co}(n,\gamma)^{60}\text{Co}$	0.0015	$0.4 \text{ eV} < E < 0.0015 \text{ MeV}$	5.27 years	
Co-Al	$^{59}\text{Co}(n,\gamma)^{60}\text{Co}$	0.0015	$E < 0.0015 \text{ MeV}$	5.27 years	

\*Denotes that monitor is cadmium shielded.

Table 2.6. Irradiation history of surveillance capsule

Month	Year	$P_j$ (MW)	$P_{\text{max}}$ (MW)	$P_j/P_{\text{max}}$	Irradiation time (days)	Decay time* (days)
12	1981	27	3565	0.007	9	679
1	1982	264	3565	0.074	31	648
2	1982	763	3565	0.214	28	620
3	1982	1223	3565	0.343	31	589
4	1982	2251	3565	0.632	30	559
5	1982	1282	3565	0.360	31	528
6	1982	2706	3565	0.759	30	498
7	1982	3389	3565	0.951	31	467
8	1982	3287	3565	0.922	31	436
9	1982	2883	3565	0.809	30	406
10	1982	3123	3565	0.876	31	375
11	1982	1366	3565	0.383	30	345
12	1982	4	3565	0.001	31	314
1	1983	3054	3565	0.857	31	382
2	1983	3495	3565	0.980	28	255
3	1983	3403	3565	0.955	31	224
4	1983	3472	3565	0.974	30	194
5	1983	3485	3565	0.978	31	163
6	1983	3160	3565	0.886	30	133
7	1983	3179	3565	0.892	19	114

$$\text{EFPS} = 3.28 \times 10^7 \text{ s} = 1.04 \text{ EFPY.}$$

\*Decay time is referenced to November 11, 1983.

Table 2.7. Results of thermal neutron dosimetry for surveillance capsule

Axial location	Saturated activity (Bq/g)		$\phi_{th}$ [n/(cm <sup>2</sup> ·s)]
	Bare	Cd-covered	
Top	$7.01 \times 10^7$	$2.79 \times 10^7$	$7.48 \times 10^{10}$
Bottom	$6.94 \times 10^7$	$2.73 \times 10^7$	$7.38 \times 10^{10}$
Average	$6.98 \times 10^7$	$2.76 \times 10^7$	$7.43 \times 10^{10}$

## 2.5 RESULT OF SAMPLE RPV ANALYSIS

The transport calculations in this particular analysis use many of the recommended "standard methods" discussed in Section 4 of this report. For example, the SAILOR Cross-Section Library and the discrete ordinates parameters are consistent with the recommended procedures. The treatment of the axial flux variation also corresponds to the method described in Section 4. For this particular analysis, the biggest difference from the recommended standard methods discussed in this report are (1) use of a generic rather than plant-specific source distribution and (2) no spectrum adjustment.

Table 2.8 gives the experimental saturated activities for various dosimeters. These are obtained from the measured activities at TOR by applying Eq. (2.4). The measured and calculated saturated activities, interpolated to the capsule centerline location, are compared in Table 2.9.

As seen in Table 2.9, the calculated activities ranged from about 12% to 40% higher than the measured values. Except for the fission dosimeters, there appears to be about a 35% to 40% bias in the calculated results. This rather poor agreement is probably due to the use of a generic source represented in the transport calculations, although this conclusion is never stated in the RPV analysis report. A similar calculation performed by this same organization for another similar unit at the same plant shows much better agreement between the calculated and measured dosimeters. Because the calculations are higher than the measurements, the calculated values are reported to be "conservative."

Also shown in Table 2.9 are the calculated and "measured" values for the integrated flux above 1 MeV in the surveillance capsule. The measured flux is actually not measured at all, but uses the measured dosimeter activities in conjunction with the calculated spectrum-average cross

sections described in Section 2.2 to obtain an adjusted capsule flux as shown in Eq. (2.5a). Finally, the fluence above 1 MeV at various positions in the RPV is given in Table 2.10 as obtained from Eq. (2.11). In this table, the results labeled "calculated" correspond to the transport calculations, while those labeled "measured" are the adjusted results obtained from Eq. (2.10). However, in this case, the adjustment factor is based only on the  $^{54}\text{Fe}$  dosimeter results, rather than the average of all dosimeters, presumably because more faith was placed on these experimental measurements. The other dosimeter measurements are not directly used in this analysis. Therefore, the adjustment factor will be:

$$\frac{(\text{ASAT})_{\text{meas}}}{(\text{ASAT})_{\text{calc}}} = \frac{3.21+10^6}{4.53+10^6} = 0.71 \quad .$$

The so-called measured fluence in Table 2.10 is obtained by multiplying the transport calculations (i.e., "calculated" results) by this scale factor.

Table 2.8. Measured saturated activities and derived fluence and fluence rates for surveillance capsule

Reaction and axial location	Measured radial location (cm)	Saturated activity at measured radial location (Bq/g)	Saturated activity interpolated to centerline (Bq/g)
<u><math>^{54}\text{Fe}(n,p)^{54}\text{Mn}</math></u>			
Top	211.68	$3.01 \times 10^6$	$3.17 \times 10^6$
Top-middle	211.68	$3.03 \times 10^6$	$3.20 \times 10^6$
Middle	211.68	$3.01 \times 10^6$	$3.17 \times 10^6$
Bottom-middle	211.68	$3.08 \times 10^6$	$3.25 \times 10^6$
Bottom	211.68	$3.11 \times 10^6$	$3.28 \times 10^6$
Average		$3.05 \times 10^6$	$3.21 \times 10^6$
<u><math>^{63}\text{Cu}(n,\alpha)^{60}\text{Co}</math></u>			
Top-middle	211.18	$3.22 \times 10^5$	$3.06 \times 10^5$
Middle	211.18	$3.24 \times 10^5$	$3.08 \times 10^5$
Bottom-middle	211.18	$3.36 \times 10^5$	$3.20 \times 10^5$
Average		$3.27 \times 10^5$	$3.11 \times 10^5$
<u><math>^{58}\text{Ni}(n,p)^{58}\text{Co}</math></u>			
Top-middle	212.18	$4.06 \times 10^7$	$4.66 \times 10^7$
Middle	212.18	$3.99 \times 10^7$	$4.58 \times 10^7$
Bottom-middle	212.18	$4.16 \times 10^7$	$4.78 \times 10^7$
Average		$4.07 \times 10^7$	$4.67 \times 10^7$
<u><math>^{237}\text{Np}(n,f)^{137}\text{Cs}</math></u>			
Middle	211.41	$3.95 \times 10^7$	$3.95 \times 10^7$
<u><math>^{238}\text{U}(n,f)^{137}\text{Cs}</math></u>			
Middle	211.41	$5.02 \times 10^6$	$5.02 \times 10^6$

Table 2.9. Comparison of measurements and calculations for surveillance capsule

Reaction	Saturated activities (Bq/g)		$\phi(E > 1.0 \text{ MeV})$ [ $\text{n}/(\text{cm}^2 \cdot \text{s})$ ]		$\phi(E > 1.0 \text{ MeV})$ ( $\text{n}/\text{cm}^2$ )	
	Meas.	Calc.	Meas.	Calc.	Meas.	Calc.
$^{54}\text{Fe}(n,p)^{54}\text{Mn}$	3.21E6*	4.53E6	6.70E10	9.44E10	2.20E18	3.10E18
$^{63}\text{Cu}(n,\alpha)^{60}\text{Co}$	3.11E5	4.11E5	7.14E10	9.44E10	2.34E18	3.10E18
$^{58}\text{Ni}(n,p)^{58}\text{Co}$	4.67E7	6.59E7	6.69E10	9.44E10	2.19E18	3.10E18
$^{237}\text{Np}(n,f)^{137}\text{Cs}$	3.95E7	4.41E7	8.46E10	9.44E10	2.77E18	3.10E18
$^{238}\text{U}(n,f)^{137}\text{Cs}^\dagger$	4.42E6	5.31E6	7.19E10	9.44E10	2.36E18	3.10E18
Average			7.24E10	9.44E10	2.37E18	3.10E18

\*Read as  $3.21 \times 10^6$ .

†U-238 adjusted saturated activity has been multiplied by 0.88 to correct for 350 ppm  $^{235}\text{U}$  impurity.

Table 2.10. Summary of neutron dosimetry results\*

Location	Current $\phi(E > 1.0 \text{ MeV})$ ( $\text{n}/\text{cm}^2$ )		EOL $\phi(E > 1.0 \text{ MeV})$ ( $\text{n}/\text{cm}^2$ )	
	Measured	Calculated	Measured	Calculated
Capsule T	$2.20 \times 10^{18}$	$3.10 \times 10^{18}$		
Vessel IR	$6.94 \times 10^{17}$	$9.78 \times 10^{17}$	$2.13 \times 10^{19}$	$3.01 \times 10^{19}$
Vessel 1/4-T	$3.85 \times 10^{17}$	$5.42 \times 10^{17}$	$1.18 \times 10^{19}$	$1.67 \times 10^{19}$
Vessel 3/4-T	$7.93 \times 10^{16}$	$1.12 \times 10^{17}$	$2.44 \times 10^{18}$	$3.43 \times 10^{18}$

\*Based on  $^{54}\text{Fe}(n,p)^{54}\text{Mn}$  reaction rate data.

NOTE: EOL fluences are based on operation at 3565 Mwt for 32 effective full-power years.

### 3. SHORTCOMINGS IN THE PRESENT RPV ANALYSIS PROCEDURE

When properly applied, the current methodology can produce estimates for the RPV fluence which are on the order of 20% accuracy. However, there are factors which can affect this accuracy. The first is the amount of rigor and effort an organization is willing to devote in order to obtain a reliable result. Thus, standards need to be established and observed. Second, the current methodology contains several inherent approximations which, under certain conditions, may introduce unacceptable inaccuracies. These should be identified and improved when necessary. Some approximations could be very questionable for extended lifetime operation. In this section, specific items are listed which could be improved to benefit the overall U.S. RPV fluence analysis effort currently being carried out by various service organizations.

#### 3.1 CROSS-SECTION SET STANDARDIZATION

Since different cross-section sets and different group structures generally produce somewhat different results, it is incumbent upon the calculator to benchmark his particular library against the results of measurements performed in simpler radiation environments or results of calculations involving cross sections commonly acknowledged as representing state-of-the-art. Laborious benchmarking of some available cross-section data and libraries has already been done. However, some of the libraries in use today are derived from extremely old ENDF/B evaluations, while others are cast into group structures that do not adequately weigh the important energy region above 1 MeV. At present, there is no conformity among the various libraries used and, as a consequence, it is difficult, if not impossible, to reconcile the results obtained by one vendor or service organization with those by another.

#### 3.2 ABSOLUTE COMPARISONS BETWEEN CALCULATED AND MEASURED DOSIMETER ACTIVITY

Strictly speaking, no absolute results are required from the transport calculations in the current methodology, since only the ratios of calculated results are used. The experimental measurements supply the normalization factor for the calculations as shown in Eq. (2.10). It has been observed that in the past, some organizations do not even report the comparisons between their unadjusted calculations and the measured dosimeter results. However, absolute comparisons between calculated and measured dosimeter activities serve as good indicators of the accuracy of the calculations. More faith may be placed in the accuracy of such calculated quantities as the lead factors when there is good agreement between the calculated and measured results. Furthermore, since there are no fluence rate measurements performed within the pressure vessel, the present method relies heavily on the discrete ordinates calculations to provide the fluence rates at the critical pressure vessel locations. Discrepancies in these calculations affect the accuracy of the estimated reactor lifetime;

but without absolute comparisons between the measurements and calculations, the present method provides no measure of the accuracy of the results, nor does it attempt to compensate for this shortcoming by incorporating a defensible safety factor for conservatism into the calculated fluence rates. As matters now stand, it is not known whether the results using the present method are generally conservative or not.

### 3.3 APPROXIMATIONS IN THE TRANSPORT CALCULATIONS

A number of approximations are inherent in the discrete ordinates transport method, such as discretization of the space, energy, and direction variables, and the finite-order Legendre expansion of the differential scatter cross section. It is important to ensure that adequate mesh, group structure, quadrature, and expansion order are used in transport calculations. There may be a reluctance among some organizations to use the proper parameters in their calculations, since cruder approximations can significantly reduce the calculational costs, but perhaps at the expense of accuracy. Standardization in the discrete ordinates parameters would help to ensure reliable results.

The flux in the RPV is a function of the three spatial coordinates. Even if only midplane parameters which vary in two coordinates are of interest, the axial leakage must be accounted for in the third dimension. The state-of-the-art in deterministic transport theory calculations is mainly limited to 2-D geometries and, thus, the 3-D effects must somehow be approximated. Usually the variation of the flux in the axial direction is represented approximately, and a 2-D transport calculation is performed to obtain the  $R\theta$  variation. Several different expressions have been used for the axial variation of the RPV flux, ranging in sophistication from (1) assuming a flat distribution, (2) assuming the same axial distribution as that of the core power, and (3) computing an axial variation using transport theory. Method (1) is especially crude and can lead to considerable error in the computed RPV fluence. Method (2) works well in many cases concerned with computing in-vessel dosimetry, as long as the axial/spatial power shape is fairly uniform throughout the core. Method (2) is not as accurate as method (3) if the axial distribution varies radially. The discrepancy can be very significant in analyzing ex-vessel (i.e., cavity) dosimetry, since the axial variation of the cavity flux can be very different from the power. The acceptable methods based on results of benchmark experiments should be identified for general use.

Several approximations exist in the current procedures for defining the core source distribution. First, in the past some organizations have used only the assembly-average power distribution, without regard for the intra-assembly variation, in representing the core source. Since the pin-wise power can vary up to a factor of four across the peripheral assemblies, this is a poor approximation. In other instances, a "generic" pinwise distribution is used, which also can be inaccurate, as illustrated in the previous section. Plant-specific data is preferable.

Another approximation in the current way of defining the core source is inherent in the use of Eqs. (2.1) and (2.4). It is tacitly assumed in Eq. (2.1) that the relative spatial distribution of the source during the period of exposure is independent of time, and that the only variation is in the absolute source normalization, which is determined from the power history. There are examples of fuel loadings in which significant variations in the midplane spatial distribution of the fission source occur as a consequence of burnup during a cycle as well as from cycle to cycle. Since the measured activities at the time of removal are reduced to saturated activities by means of Eq. (2.4), this approximation in the source description can have a direct impact on the accuracy of the derived fluence rates in Eq. (2.5). In cycles for which there is a significant time-dependent variation in the spatial power distribution, it may be necessary to employ a more sophisticated method than simply using the time-averaged distribution in the transport calculations. This approximation mainly affects the predicted activities for the short-lived dosimeter products which are most sensitive to the power distribution near the time of removal, and for reactor cores in which the power fraction produced by the peripheral assemblies changes a large amount during the period of irradiation.

#### 3.4 MULTI-CYCLE ANALYSIS

If the power distribution does not behave very much differently from cycle to cycle, then a representative source distribution can be obtained by averaging over the different cycles. However, if the power distribution in the outer assemblies varies significantly in different cycles, such as between a conventional and low-leakage core loading, then separate transport calculations should be performed for each cycle. An alternative to this potentially expensive approach is described in Section 4.4.3.

#### 3.5 CONSOLIDATION OF MEASURED AND CALCULATED RESULTS

In the current methodology, the measured dosimeter activities are used to scale the calculated RPV integrated flux as shown in Eq. (2.10). Thus the measured and calculated results are consolidated through the adjustment factor of

$$\left\langle \frac{(ASAT)_{\text{meas}}}{(ASAT)_{\text{calc}}} \right\rangle .$$

Note that no spectrum adjustment is made using Eq. (2.10) -- only the overall magnitude of the calculated flux is changed by the adjustment factor. In reality, the energy distribution as well as the magnitude of the calculated flux has uncertainties associated with it, and should be affected by consolidation with the experimental results. This spectrum adjustment, often called "unfolding," is not performed with the current methodology. Spectral adjustment will be especially important if parameters such as dpa (displacements per atom) rather than gross integrated flux are used to monitor radiation damage.

Equation (2.10) also implicitly assumes that the adjustment made to calculated results at the surveillance location is appropriate for all locations in the RPV. This assumption essentially rules out any adjustment to the lead factor; i.e., it is assumed that the calculated lead factor is correct so that errors in the transport calculation are the same in the RPV as in the surveillance location.

The calculational error actually varies spatially, especially in penetrating the RPV. If cavity dosimetry is used exclusively for surveillance, then the discrepancy between the measured and calculated dosimeter activities may be considerably greater than the error in the transport calculation at the inner radius of the RPV. The adjustment factor as defined in the current methodology will be inappropriate in this case.

## 4. RECOMMENDED IMPROVEMENTS IN RPV TRANSPORT ANALYSIS PROCEDURES

### 4.1 OVERVIEW

In this section, the areas identified and described in the previous section, and improvements are suggested to the present methods of computing RPV fluence and surveillance dosimeter activities. These improvements could be especially beneficial in analyzing extended reactor lifetime operation since the RPV surveillance program under these conditions will probably require a reduced uncertainty in the estimated fluence. At the same time, the transport calculations will be addressing problems which are not routinely faced in the present RPV analysis; e.g., modified core designs, exclusive use of cavity dosimetry for surveillance monitoring, etc. Thus, it is desirable to have available general methods which can be more easily applied to future conditions. In addition, it is important to establish a standard procedure and data base for performing RPV fluence calculations, since this would help to assure the quality of the results obtained by various organizations. Therefore, much of this section addresses the question of standardization as well as actual improvement and generalization of techniques. The standardized methods and procedures should be based on conclusions obtained from their application to the extensive collection of benchmark experiments which have been completed or are in progress. Some of the areas covered in this section are (1) standardization of nuclear data library, (2) standardization of various discrete ordinates parameters, (3) improvements in the methods used to treat the various space- and time-dependent effects on RPV fluence and surveillance dosimetry, and (4) least squares adjustment to combine the results of the transport calculations with the dosimeter measurements. In area (3), improvements in describing the spatial distribution of the core source, in treating the time-dependent variation in the source shape and magnitude, and in "synthesizing" a 3-D flux from lower dimensional calculations are considered. Many of the recommendations presented here have evolved from considerable experience in analyzing research and power reactor benchmarks.<sup>14,15,19,20,26,28,29,33</sup>

### 4.2 STANDARDIZED NUCLEAR DATA

A standardized set of nuclear data should be established and maintained for RPV fluence analysis. A nationally available, multigroup cross-section library which is suggested by the NRC as a standard would provide quality assurance, as well as facilitate inter-comparison of results obtained by different organizations. It is also desirable for the library to be available to other countries performing RPV calculations since this would encourage international cooperation in this area. The multigroup data must (1) include interaction cross sections for the discrete ordinate transport calculations, fission source spectra, and important dosimeter activation cross sections; (2) be validated in benchmark experiments; (3) contain gamma-ray production and transport cross sections as part of a coupled set for consistent use in gamma-ray heating applications that are not of interest in the present analysis;

(4) have an adequate number of neutron groups above 0.1 MeV; (5) be well documented and easily accessible to all organizations, and (6) be compatible with transport and adjustment codes used in the RPV analysis. Organizations which desire to use data other than the standard library should show that their data perform equally well on established benchmark experiments. Periodic improvements could be made to the standard library as improved nuclear data becomes available.

The ELXSIR<sup>30</sup> or SAILOR<sup>10</sup> Libraries perhaps come closest to meeting all the required specifications. The 56-neutron group ELXSIR Library contains 37 groups above 0.1 MeV but as yet contains no gamma-ray groups or an adequate thermal-neutron group. It does, however, satisfy the remaining criteria. The SAILOR Library consists of 47 neutron groups, of which 26 lie above 0.1 MeV, and two adequate thermal-neutron groups. It is also a coupled library, containing 20 gamma-ray groups. However, the dosimetry cross sections are not as accurate as those of the ELXSIR Library, which have been updated.<sup>13,31</sup> It is also not compatible with the LEPRICON adjustment code (see Section 4.5), if that is to be used in the analysis. Both libraries are readily available from the Oak Ridge National Laboratory.

There is a common shortcoming in both libraries, which should be modified in the standard library. First, it has been previously observed in benchmark experiment analyses that the iron inelastic cross section in ENDF/B-IV appears to be too large and tends to over-attenuate neutrons passing through thick steel regions, such as the RPV. Recently, Fu has performed a new evaluation of the iron cross section which appears to give better agreement between transport calculations and measurements of neutron penetration through iron.<sup>12</sup> However, the new iron data have not been thoroughly tested against RPV benchmark and power reactor measurements.<sup>29,33</sup> It is recommended that the new iron cross sections be validated as soon as possible and, if improved results continue to be obtained, be made part of the standard RPV cross-section library.

In summary, it is recommended that a modified version of the ELXSIR or SAILOR Cross-Section Library be developed and designated to be the nation standard multigroup data for RPV fluence calculations. The library would be modified by implementing and testing the new Fu evaluation of the iron inelastic cross-section data.

#### 4.3 STANDARDIZED DISCRETE ORDINATES METHODOLOGY

Transport calculations of the RPV fluence are almost universally performed in the U.S. with a two-dimensional discrete ordinates transport code such as DOT.<sup>6</sup> These codes place many options and approximations at the discretion of the user. This approach provides much flexibility, but also provides the opportunity for the user to make a poor choice of options, resulting in an inaccurate calculation of the RPV fluence. In order to provide adequate approximations in the transport calculations, it is recommended that the following procedures be proposed for RPV fluence calculations. (Many calculators are already using these procedures.)

1. Use a  $P_3$  Legendre expansion of scattering cross sections.
2. Use an  $S_8$  (48 directions) fully symmetrical quadrature.\*
3. Use the theta-weighted or weighted difference flux extrapolation model.
4. Use a point flux convergence of 0.001. Make sure that the calculation is not terminated before convergence is obtained due to an insufficient number of inner iterations. Usually 15 iterations are more than sufficient.
5. Compute the RPV fluence and dosimeter activities by combining results from an  $R\theta$  transport calculation for the radial and azimuthal dependence with an appropriate axial distribution function. A second transport calculation in RZ geometry may be required to obtain the axial distribution, if the axial flux shape changes significantly as a function of radius (e.g., in the cavity). This is discussed in Section 4.4.4.
6. Make the  $R\theta$  mesh fine enough to adequately represent the irregular core boundary (since the irregular nature of the core causes azimuthal variations in the RPV fluence). Experience in benchmark experiments has shown that this generally requires 40 to 80  $\theta$  intervals not necessarily evenly spaced, over a one-eighth core. Using the "variable-mesh" capability in DOT-4 is a considerable aid in determining an appropriate radial mesh. As a rule of thumb, the core midplane area as defined by the  $R\theta$  mesh should be within 0.5% of the true value. The steel baffle surrounding the core of a PWR should be explicitly included in the DOT model, as should the surveillance capsule holder in all reactors.
7. Use at least three intervals for every inch in water and three intervals for every two inches in steel for the radial mesh.

#### 4.4 TREATMENT OF SPACE- AND TIME-DEPENDENT EFFECTS

The scalar flux incident on a RPV actually varies in terms of five independent variables: three spatial coordinates ( $R, \theta, Z$ ), energy (group), and time. The spatial distribution of the flux is a function of the in-core and ex-core reactor geometry and of the core source distribution. The magnitude and energy spectrum of the RPV flux varies with time during a given cycle due to changes in the core source with burnup, control-rod

---

\*For narrow cavities and detectors considerably removed from the reactor midplane, a finer quadrature may be required to handle the streaming properly.

movement, power swings, etc. There may also be significant cycle-dependent variations arising from modifications to the fuel loading pattern each cycle.

Thus, there are several space- and time-dependent effects which impact the determination of the RPV fluence in a power reactor. The methodology established for RPV transport calculations should include the following:

1. method to obtain the absolute, space-dependent source distribution (at a given instant in time);
2. method to account for time-dependent variations in the source, within a given cycle;
3. method to account for cycle-to-cycle variations in the source; and
4. method to synthesize a 3-D flux distribution from lower dimensional transport calculations.

Procedures for addressing each of these areas are outlined in the following section.

#### 4.4.1. Space-Dependent Source Distribution

The space-dependent neutron source density decreases substantially across the outer row of assemblies in a light water reactor (LWR).<sup>15</sup> Since the neutron importance for contributing to the RPV fluence is largest near the core periphery, the pin-wise variation of the power density within the outer assemblies can have a noticeable affect on the RPV fluence.

Therefore, it is recommended that the intra-assembly (i.e., pin-wise) as well as the inter-assembly (i.e., assembly-wise) power distribution be considered in defining the absolute source used in transport calculations of the RPV flux. A reasonable procedure is to utilize the plant-specific relative pin-power distribution for the one-quarter core, which is computed each cycle from core physics analysis with a diffusion theory code such as PDQ<sup>16</sup> for PWRs or a multi-pin code such as CASMO<sup>17</sup> for Boiling Water Reactors (BWRs). The one-quarter core relative pin power for the peripheral assemblies can be normalized on an assembly-wise basis to obtain the absolute source distribution at any instant in time. The absolute assembly powers can be obtained from the actual plant operating data (in-core detector measurements), augmented if necessary with results from 3-D nodal calculations, for several exposures during the cycle. The final results of this procedure will be an absolute source distribution defined for each pin within the outer row of assemblies; e.g., depending on the particular type of PWR, there will be 15 X 15 or 16 X 16 or 17 X 17 source-density values within each peripheral assembly. The intra-assembly power distribution for assemblies not on the periphery is not very important. An adequate approximation is to simply use a flat distribution (average assembly power density) within each interior assembly. Thus, the one-quarter core source distribution will be an assembly-wise constant for the interior region and show a pin-wise

variation in the peripheral elements. A new space-dependent source must be generated for each time period considered in the activity calculation, as discussed in the following section.

There is a complication encountered in implementing the properly defined, one-quarter core source distribution into the actual transport calculations. The pin-wise core source is generally defined in a rectangular (one-quarter core) coordinate system, whereas the RPV transport calculations are performed in cylindrical ( $R\theta$  and  $RZ$ ) coordinates. Therefore, it is necessary to transform the rectangular source into cylindrical coordinates. This requires laborious interpolation and re-normalization to ensure an accurate source distribution for the DOT  $R\theta$  and  $RZ$  transport calculations. It is recommended that a standard code (or codes) be designated for this operation and be made available to organizations that perform RPV fluence analysis. The DOTSOR code,<sup>18</sup> which was originally developed as part of the LEPRICON<sup>19</sup> system, is an example of such a program.

#### 4.4.2. Time-Dependent Variations in the Source Over a Cycle

The core source changes its spatial and energy shape as well as its magnitude as the reactor operates. Usually, the source shape varies slowly within a given cycle, whereas the magnitude can change more rapidly in response to changes in the power level. Changes in the core source affect the flux incident on the RPV as well as the activation rate of surveillance dosimetry.<sup>19</sup>

Often the time-dependent variations are slow and regular, and in these cases the time-averaged distribution over the cycle may be employed. In some cases, however, due to the burnout of burnable poisons or severe changes in control-rod patterns, the cycle-averaged distributions may not be appropriate. This can be especially true for short-lived dosimeter activation products [such as  $^{58}\text{Ni}(n,p)^{58}\text{Co}$ ] which are most affected by the power distributions present a few months prior to capsule removal, rather than the cycle-average distribution. In this section, new methods which will more rigorously account for the space-time source effects are presented to treat the time-dependent source effects on both RPV fluence and dosimeter activation. This approach should be used whenever the conventional method of using the time-averaged source is not appropriate.

Assume that the space-energy source distribution at some time  $t$  is known and given by  $Q(r,E,t)$ . For example, the absolute power distribution is found by combining pin-wise and assembly-wise power distributions at time  $t$  as described in the previous section. The power distribution can be converted to a source distribution by multiplication by an appropriate conversion factor. This conversion factor has been found to vary slightly with burnup - the following correlation has been derived:<sup>18</sup>

$$C(B) = (A_0 + A_1B + A_2B^2 + A_3B^3 + A_4B^4) \times 10^{-5} ,$$

where  $C$  = power-to-source conversion factor [(neutron/s)/MW];

$B(t) = \ln$  [burnup (MWD/T)] of peripheral assemblies at time  $t$ ; and

$A_0, A_1, A_2, A_3,$  and  $A_4$  are given, respectively, by the constants  $-9.8135, 8.7814 \times 10^{-1}, -1.6286, 1.3184 \times 10^{-1},$  and  $-3.8863 \times 10^{-3}.$

This correlation is valid for burnup  $>500$  MWD/T. For values  $<500$  MWD/T, a conversion factor of  $7.708 \times 10^{16}$  is appropriate. The above correlation does not account for the burnup dependence of the energy distribution.

The energy distribution of the source is equal to an effective fission spectrum. The fission spectrum tends to harden slightly with time, due to buildup of  $^{239}\text{Pu}$  and depletion of  $^{235}\text{U}$ ; however, this effect is often ignored, and a pure  $^{235}\text{U}$  spectrum is used, such as given in ENDF/B-V. To be more rigorous, an average fission spectrum is considered for the peripheral assemblies at time  $t$ , designated  $\bar{\chi}(E,t)$  which is a weighted combination of the  $^{235}\text{U}$  and  $^{239}\text{Pu}$  spectra appropriate for the peripheral assemblies. Thus, the time-dependent source is equal to

$$Q(\mathbf{r}, E, t) = C \bar{\chi}(E, t) P(\mathbf{r}, t) \quad , \quad (4.1)$$

where  $P(\mathbf{r}, t)$  is the absolute power density distribution. Often it is useful to express  $P(\mathbf{r}, t)$  as the product of a shape distribution (relative power) and the total power  $P_T(t)$ :

$$P(\mathbf{r}, t) = R(\mathbf{r}, t) \cdot P_T(t) \quad (4.2)$$

$$\text{where } R(\mathbf{r}, t) = \frac{P(\mathbf{r}, t)}{P_T(t)} \quad .$$

The advantage to expressing the power distribution in this form is that the shape distribution  $R$  usually varies more slowly than the total power  $P_T(t).$ <sup>20</sup>

Having obtained the time-dependent source distribution, the manner in which it can be used in computing RPV fluence and dosimeter activation is determined. Consider first the question of RPV fluence. The space- and energy-dependent fluences at time  $t$  are equal to

$$\phi(r, E, t) = \int_0^t \phi(r, E, t') dt' \quad (4.3)$$

where the time-dependent scalar flux is computed from the time-dependent angular flux,

$$\phi(\mathbf{r}, E, t) = \int_{4\pi} \psi(\mathbf{r}, E, \hat{\Omega}, t) d\hat{\Omega} \quad . \quad (4.4)$$

The angular flux obeys the transport equation

$$B\psi(r, E, \hat{\Omega}, t) = Q(r, E, t) \quad . \quad (4.5)$$

In this equation, let "B" stand for the Boltzman transport operator, in order to simplify notation.

The fluence is related to the angular flux by

$$\phi(r, E, t) = \int_{4\pi} \int_0^t \psi(r, E, \hat{\Omega}, t') dt' d\hat{\Omega} = \int_{4\pi} \phi(r, E, \hat{\Omega}, t) d\hat{\Omega} \quad , \quad (4.6)$$

where  $\phi(r, E, \hat{\Omega}, t)$  is the angular fluence. Thus, once the angular fluence is known, the (scalar) fluence is easily computed.

The equation obeyed by the angular fluence is obtained by integrating Eq. (4.5) from  $t'=0$  to  $t'=t$ :

$$B\phi(r, E, \hat{\Omega}, t) = \int_0^t Q(r, E, t') dt' \quad . \quad (4.7)$$

From Eq. (4.7), it is seen that the angular fluence distribution obeys the Boltzman transport equation, with a time-integrated fixed source. The average flux throughout the system during the time period (0,T) is thus equal to

$$\bar{\phi}(r, E) = \frac{\bar{\phi}(r, E, T)}{T} \quad . \quad (4.8)$$

This average flux will be used later in determining the dosimeter activation.

Hence, a single transport calculation is required to obtain a two-dimensional mapping of the RPV fluence, regardless of the time-dependent variation in the source because only the integrated source affects the fluence, not the actual time dependence. All neutrons which strike the RPV are scored equally, regardless of the time they hit the vessel. Unfortunately, this is not the case for dosimeter activation.

The activities of the various surveillance dosimeters build up with time until eventually they "saturate," if the the reactor is operated long enough. The neutrons which strike the various dosimeters at times near TOR are more important than those which strike near the beginning of life, because the radioactive dosimeter products created early will have a higher probability of decaying before being removed from the reactor. Hence, the source distribution at later times should be weighted more heavily than near the beginning of life. In the following development, a rigorous relation is derived between the space- and time-dependent source and the time-dependent dosimeter activities.

The time-dependent activity  $A_i$  of a dosimeter foil "i" obeys the following differential equation

$$\frac{d}{dt} A_i(t) = \lambda_i R_i(t) - \lambda_i A_i(t) \quad (4.9)$$

where  $R_i$  = dosimeter reaction rate at time  $t$

$$R_i = N_{oi} Y \int_0^{\infty} \phi(r_i, E, t) \sigma_i(E) dE \quad (4.10)$$

The parameters in Eq. (4.10) have the same meanings as given in Sect. 2.0, and  $r_i$  indicates the spatial position of the dosimeter  $i$ . Note that the flux at the dosimeter location is time-dependent due to the time varying core source. The core source distribution can change in overall magnitude as well as in its relative space and energy distribution. Even if the total reactor power output is kept constant, the flux at the dosimeter location may be time-dependent if the spatial distribution of the power density changes.

The solution to Eq. (4.9) is (assuming no initial activity at  $t=0$ )

$$A_i(t) = \lambda_i \int_0^t e^{\lambda_i(t-t')} R_i(t') dt' \quad (4.11)$$

Evaluating Eq. (4.11) at  $t=T$ , the time of removal (TOR), and substituting Eq. (4.10) for  $R_i$  gives

$$A_{i,TOR} = N_{oi} Y \int_0^{\infty} \sigma_i(E) \int_0^T \lambda_i e^{\lambda_i(t'-T)} \phi(r_i, E, t') dt' dE \quad (4.12)$$

Eq. (4.12) is an exact expression for the TOR activity of dosimeter  $i$ . Often the time-dependent core source is slowly varying with time and, therefore, can be approximated as piece-wise constant, i.e.,

$$Q(r, E, t) = Q_j \quad (4.13a)$$

so that

$$\phi(r_i, E, t) = \phi_j(r_i, E) \quad , \text{ for } t_{j-1} < t < t_j \quad ; \quad j=1, J \quad (4.13b)$$

where  $t_0=0$  and  $t_J = T$ .

The value of  $J$  is equal to the number of time intervals used to represent the time-dependent source variation. Using the approximation in Eq. (4.13b), Eq. (4.12) becomes

$$A_{i,TOR} = N_{oi} Y \int_0^{\infty} \sigma_i(E) \sum_{j=1}^J \phi_j(r_i, E) (1 - e^{-\lambda_i T_j}) e^{-\lambda_i(T-t_j)} dE \quad (4.14)$$

Assuming that Eq. (4.13) is a good approximation (as it usually is), Eq. (4.14) will give an accurate estimate for the dosimeter activity. However, notice that in order to evaluate Eq. (4.14), the value of the flux at each of the time intervals must be known. This would involve performing DOT transport calculations at each of the  $J$  time steps, using the appropriate source distribution for the time interval.

In order to avoid these expensive computations, a simplifying assumption is always made in the current methods. These current methods effectively designate a time-independent, "nominal flux" distribution to be  $\phi_N(\mathbf{r}, E)$ . Only a single transport calculation is required to obtain the nominal flux. The source for this nominal transport calculation is usually normalized to full power; but determination of the spatial distribution appears to be somewhat vague. A middle-of-cycle (MOC) distribution is sometimes used, or sometimes the cycle-average or some other shape is selected. Since the power distribution changes with time, no single shape is correct for all times. Using the nominal flux Eq. (4.14) can be re-arranged to

$$A_{i, \text{TOR}} = N_{oi} Y \int_0^{\infty} \sigma_i(E) \phi_N(\mathbf{r}_i, E) \sum_{j=1}^J \frac{\phi_j(\mathbf{r}_i, E)}{\phi_N(\mathbf{r}_i, E)} (1 - e^{-\lambda_i T_j}) e^{-\lambda_i (T - t_j)} dE \quad (4.15)$$

No approximations are made in going from Eq. (4.14) to Eq. (4.15); however, Eq. (4.15) still requires knowing  $\phi_j$ , the flux at each time step. The present methods approximate the flux ratio appearing in the summation of Eq. (4.15) by

$$\frac{\phi_j(\mathbf{r}_i, E)}{\phi_N(\mathbf{r}_i, E)} = \frac{P_j}{P_N} \quad , \quad (4.16)$$

where  $P_j$  is the reactor power level at time step  $j$ , and  $P_N$  is the nominal (e.g., full power) level. This approximation amounts to assuming that the space and energy shape of the flux is constant. Only the flux normalization, as fixed by the total power level, changes with time. This assumption is rigorous only if the relative power distribution is time independent, i.e., if the power density is separable in space and time. Substitution of Eq. (4.16) into Eq. (4.15) results in Eq. (2.1), which is the expression currently used to compute dosimeter activities. It has been shown in some cases that using the total power instead of local power variations can cause up to 20% error in some computed activities.<sup>21</sup>

A more rigorous and accurate method of computing activities should take into account changes in the shape of the core source as well as in its overall magnitude. Such a method has been developed based on using an adjoint transport calculation. Recall that the difficulty with using the "exact" expression in Eq. (4.14) is the expense in evaluating the term  $\int_0^{\infty} \sigma_i(E) \phi_j(\mathbf{r}_i, E) dE$ .

This term can be expressed in terms of angular flux as

$$\int_0^{\infty} \sigma_i(E) \phi_j(\mathbf{r}_i, E) dE = \int_0^{\infty} \sigma_i(E) \int_{4\pi} \psi_j(\mathbf{r}_i, E, \hat{\Omega}) d\hat{\Omega} dE, \quad (4.17)$$

and thus requires solving the transport equation at each time step for which the source distribution changes; i.e., it is necessary to solve

$$B\psi_j(\mathbf{r}, E, \hat{\Omega}) = Q_j(\mathbf{r}, E) \quad \text{for } j=1, J. \quad (4.18)$$

Using the adjoint approach, it is possible to avoid solving the transport equation at each time step. Instead, one solves a single adjoint transport equation for dosimeter "i" corresponding to

$$B^*\psi_i^*(\mathbf{r}, E, \hat{\Omega}) = \sigma_i(E) \delta(\mathbf{r}-\mathbf{r}_i) \quad , \text{ for dosimeter } i \quad (4.19)$$

where  $B^*$  is the adjoint transport operator,  $\psi^*$  is the adjoint flux, and  $\delta(\mathbf{r}-\mathbf{r}_i)$  is the Dirac delta function. DOT will easily solve the adjoint transport equation if the appropriate input parameters are specified.

It can be shown by using properties of adjoint operators that<sup>22</sup>

$$\int_0^\infty \int_{4\pi} \sigma_i(E) \psi_j(\mathbf{r}_i, E, \hat{\Omega}) d\hat{\Omega} dE = \langle Q_j(\mathbf{r}, E) \psi_i^*(\mathbf{r}, E, \hat{\Omega}) \rangle \quad , \quad (4.20)$$

where the brackets  $\langle \rangle$  are shorthand notations for integration over  $\mathbf{r}$ ,  $E$ , and  $\hat{\Omega}$ . Substituting Eq. (4.20) into Eq. (4.19) and then substituting this result into Eq. (4.14) gives a rigorous expression for the activity of dosimeter i:

$$A_{i, \text{TOR}} = N_{oi} Y \sum_{j=1}^J \langle Q_j \psi_i^* \rangle (1 - e^{-\lambda_i T_j}) e^{-\lambda_i (T - t_j)} \quad . \quad (4.21)$$

Equation (4.21) is exactly equivalent to Eq. (4.14), but it requires only a single adjoint calculation instead of a forward calculation for each time step.

However, there is a drawback to using the adjoint approach. Note that the source on the right-hand side of Eq. (4.19) depends on the dosimeter activation cross section and, therefore, a separate adjoint equation is required for each dosimeter. If many different dosimeters are used, then the adjoint calculations also will become expensive. Fortunately, a very powerful and accurate approximation has been discovered which avoids this difficulty.<sup>20</sup>

It has been found that the ratio of the reaction rates of various dosimeters is very insensitive to the core source distribution, i.e., at time step j

$$\frac{R_{k,j}}{R_{i,j}} = \frac{\int_0^\infty \sigma_k(E) \phi_j(\mathbf{r}_k, E) dE}{\int_0^\infty \sigma_i(E) \phi_j(\mathbf{r}_i, E) dE} = \text{constant for all } j \quad . \quad (4.22)$$

This relation is valid because the reaction rate ratio depends on the flux energy spectrum at the dosimeter points and the flux spectral shape does not change much with time because it is insensitive to the spatial distribution of the core source. Therefore, a single forward calculation can be used to estimate the reaction rate ratios. Recall that the average flux given in Eq. (4.8) is obtained rigorously from the calculation of the RPV fluence and, therefore, is the obvious choice to use in evaluating the reaction rate ratios.

In order to evaluate the activities of the various dosimeters, taking into account the time-dependent variation in the core source, the following procedure can be used:

1. choose a "reference dosimeter" which has an intermediate reaction threshold - either  $^{54}\text{Fe}(n,p)$  or  $^{58}\text{Ni}(n,p)$  serves well for this purpose. The index "i" will correspond to the reference dosimeter;
2. perform a single adjoint calculation for this reference dosimeter, which produces the adjoint function  $\psi_i^*$ ;
3. compute the reaction rate ratios of the various dosimeters, relative to the reference dosimeter

$$\frac{R_k}{R_i} = \frac{\int_0^\infty \sigma_k(E) \bar{\phi}(t_k, E) dE}{\int_0^\infty \sigma_i(E) \bar{\phi}(t_k, E) dE} \quad (4.23)$$

where  $\bar{\phi}$  is the time-average flux as found in the forward RPV fluence calculation; and

4. compute the activity at TOR of any dosimeter "k" by evaluating

$$A_{k, \text{TOR}} = \left( \frac{R_k}{R_i} \right) N_{0k} Y_k \sum_{j=1}^J \langle Q_j \psi_i^* \rangle (1 - e^{-\lambda_k T_j}) e^{-\lambda_k (T - t_j)} \quad (4.24)$$

In summary, the procedure described here for addressing the effects of time-dependent source variations on RPV fluence and surveillance dosimeter activities requires performing (1) one forward transport calculation, using the time-integrated source distribution and (2) one adjoint transport calculation, using the reference dosimeter cross section as a source term.

With these results, the RPV fluence and the reference dosimeter activity can be calculated rigorously taking into account changes in the source shape as well as magnitude. The activities of the other dosimeters are computed very closely by using the reaction-rate scaling as shown in Eq. (4.24). The scaling approximation appears to be quite accurate and has been found to introduce errors of only about 3% into the computed dosimeter activities for typical time-dependent source variations.<sup>20</sup> The computer program TIMEPATCH in the LEPRICON system evaluates a special form of Eq. (4.24).<sup>23</sup>

#### 4.4.3 Cycle-Dependent Source Variations

The time-dependent behavior of the core source may vary from cycle to cycle. In theory, after the equilibrium fuel management program is established, each cycle will behave the same. In reality, however, there are usually fuel loading and operational variations which will continue to make each cycle unique. The recent trend toward low-leakage core configurations results in significant cycle-wise source variations.<sup>24</sup>

Therefore, each cycle for which the surveillance dosimeter is in the reactor should be considered in the transport calculations. It is often adequate to lump several cycles together which have similar power distributions by averaging the respective sources. A transport calculation must then be performed for each set of cycles, and the results combined in a manner which accounts for the radioactive decay of the dosimeter. If the adjoint methodology described in the previous section on treating time-dependent source variations is followed, then multi-cycle analysis is very straight-forward. Only one additional complication may be introduced by considering each cycle of irradiation. An additional adjoint transport calculation may now be required if there is a change in the materials geometry (such as the introduction of a partial length shield) that accompanies the new cycle loading. Also, every time a set of surveillance dosimetry is removed from the core and analyzed, a single forward calculation will be required to obtain the accumulated RPV fluence over the time spanned by the dosimetry. Usually, the dosimetry is only removed every few cycles, so that a transport calculation is not needed for every cycle unless a materials change is made.

For example, suppose a particular set of dosimeters has been placed in a reactor at the BOL and is being removed after cycle L to be analyzed. Let  $m$  be the cycle index and assume that there are  $J$  time-intervals within each cycle, during which the source distribution changes. In order to analyze these dosimeters, a single forward calculation is performed using the time-integrated source given by

$$Q(r,E) = \int_0^T Q(r,E,t) dt = \bar{Q}(r,E)T \quad (4.25)$$

where  $T = \text{TOR} = \text{time until end of cycle } L$ .

The time integral is equal to

$$\int_0^T Q dt = \sum_{m=1}^L \sum_{j=1}^J Q_{mj}(r,E) \Delta t_j \quad (4.26)$$

where  $Q_{mj}$  = source distribution at time step  $j$ , within cycle  $m$ , and

$\Delta t_j$  = length of the  $j$ th time interval.

If the source distribution is virtually unchanged over several cycles, then the summation in Eq. (4.26) will reduce accordingly. The expression in Eq. (4.24) for the dosimeter activity is treated analogously, by replacing the sum over  $j$  with a double sum over  $j$  and  $m$ .

An alternative procedure may be followed if a complete fluence mapping over the RPV is not required to locate the absolute position of the peak flux. In this case, a new forward transport calculation need only be made following a major source distribution change such as in going from a high-leakage to a low-leakage core fuel management scheme, or following a significant change in the materials geometry. This alternative procedure treats the RPV group fluxes as simply responses which scale in the same manner as the dosimeter activities do in Eq. (4.23).<sup>20</sup> Instead of the time-averaged flux  $\phi$  in Eq. (4.23), a midcycle flux distribution calculated by using a midcycle source distribution for a single representative cycle in DOT may be substituted. The dosimeter activities are still calculated using Eq. (4.24), and the accumulated group fluences by

$$\phi_{g, \text{TOR}} = \left( \frac{\phi_g}{R_i} \right) \sum_{j=1}^J \langle Q_j \psi_i^* \rangle T_j \quad (4.27)$$

where  $\phi_g$  is the group flux calculated using the midcycle source.

#### 4.4.4 Three-Dimensional Flux Synthesis

Although a few 3-D discrete ordinates codes are now beginning to appear, the cost of running these codes on a routine basis seems prohibitive. Furthermore, in most problems encountered in RPV fluence analysis, the axial distribution of the core power can be reasonably assumed to be a smoothly varying function which only changes slightly among the peripheral assemblies, the most important region for contributing to the RPV fluence. Therefore, a detailed 3-D transport solution is not warranted; instead a type of flux "synthesis" approximation is adequate.

To evaluate the RPV fluence and dosimeter activities, the 3-D transport equation shown in Eq. (4.5) needs to be solved. In this equation,  $\mathbf{r}$  specifies the spatial position which in general is determined in 3-D cylindrical geometry by the coordinates,

$$\mathbf{r} = (R, \theta, Z) \quad (4.28)$$

Several different methods have been used to approximate the 3-D RPV flux distribution by using results of lower dimensional (2-D and 1-D) calculations. The two most accurate methods - which are used today with several variations - will be called in this report (1) the midplane method and (2) the single-channel synthesis method. The most important common factor of the two approaches is the use of two 2-D transport calculations to synthesize a 3-D flux distribution. Some less accurate techniques use a single 2-D  $R\theta$  transport calculation, to which a "generic" (i.e., pre-determined) axial distribution function is applied. Although both the midplane and synthesis approaches can produce accurate results, the

single-channel synthesis method is preferred over the midplane method because in the synthesis technique the axial leakage is treated rigorously. The midplane method will be described first.

In the midplane method, a 3-D flux is synthesized from the results of R $\theta$  and RZ transport calculations, using the expression (the group index is suppressed for simplicity):

$$\phi_M(R, \theta, Z) = \phi_O(R, \theta) \frac{\phi_{RZ}(R, Z)}{\phi_{RZ}(R, Z=0)} \quad (4.29)$$

where  $\phi_M(R, \theta, Z)$  = 3-D synthesized flux, obtained with the midplane method;

$\phi_O(R, \theta)$  = flux obtained from a 2-D R $\theta$  transport calculation of the reactor midplane (defined to be  $Z=0$ ); and

$\phi_{RZ}(R, Z)$  = flux obtained from a 2-D RZ transport calculation of the reactor.

Note that, if  $\phi_O$  is a good estimate for the midplane flux, then Eq. (4.29) will preserve the value of the flux at  $Z=0$  (i.e., the midplane). The main difficulty with this approach is in treating the axial leakage in the midplane R $\theta$  calculation of  $\phi_O(R, \theta)$ . Either a buckling approximation must be used or appropriate axial leakage factors must be obtained. Both of these approaches are approximate. Note that the R $\theta$  source used in the calculation of  $\phi_O$  must be input per unit height. If the axial leakage is treated correctly, or is negligible, then the midplane synthesis method should produce accurately synthesized fluxes, especially near  $Z=0$ .

The single-channel synthesis expression is similar to Eq. (4.29), except it is defined in terms of R $\theta$ -, RZ-, and R-"channel fluxes," which correspond to integrals of the true R,  $\theta$ , Z 3-D flux over the omitted coordinates, respectively.<sup>25</sup> For example, the R $\theta$ -channel flux is equal to the integral of the 3-D (i.e., R,  $\theta$ , Z) flux over the axial coordinate, Z. The RZ-channel flux is the integral over  $\theta$ , and the R-channel flux has been integrated over both  $\theta$  and Z. The channel fluxes are obtained by solving the transport equation in the respective 2-D and 1-D geometries; e.g., the R $\theta$ -channel flux is obtained by solving an R $\theta$  transport equation, etc. The single-channel synthesis method is described below.

The channel fluxes are defined as follows:

$$\phi_{R\theta}(R, \theta) = \int_{-\infty}^{\infty} \phi(R, \theta, Z) dZ = \text{R}\theta\text{-channel flux,} \quad (4.30)$$

$$\phi_{RZ}(R, Z) = \int_0^{2\pi} \phi(R, \theta, Z) d\theta = \text{RZ-channel flux, and} \quad (4.31)$$

$$\phi_R(R) = \int_{-\infty}^{\infty} \int_0^{2\pi} \phi(R, \theta, Z) d\theta dZ = \text{R-channel flux.} \quad (4.32)$$

Note that the following relations among the channel fluxes must hold for each group:

$$\int_0^{2\pi} \phi_{R\theta} d\theta = \int_{-\infty}^{\infty} \phi_{RZ} dZ = \phi_R \quad (4.33)$$

The "synthesized flux" is defined to be a function of the three variables  $R, \theta, Z$  which is given by the following relation:

$$\phi_{\text{SYN}}(R, \theta, Z) = \frac{\phi_{R\theta}(R, \theta) \phi_{RZ}(R, Z)}{\phi_R(R)} \quad (4.34)$$

Note the similarity to Eq. (4.29). The above expression has a number of desirable properties.

The single-channel synthesis approximation has been shown to have the following features:<sup>25</sup>

1. gives the exact 3-D distribution if the flux is separable in  $Z$ ,
2. gives the exact 3-D distribution if the flux is separable in  $\theta$ ,
3. always gives the exact value for the axially integrated flux at all  $R$  points,
4. always gives the exact value for the azimuthally integrated flux at all  $R$  points, and
5. is simple and economical to evaluate once the channel fluxes are available.

In reality, of course, the channel fluxes cannot be computed from Eqs. (4.30) through (4.32), since the true 3-D flux is not known; therefore, an alternate method must be used for computing 2-D and 1-D channel fluxes.

It can be shown that the  $R\theta$ -channel flux obeys an equation which has the identical form as the standard  $R\theta$  transport equation solved by transport codes such as DOT-IV; however, the source is integrated axially, and the cross sections are weighted by the axial flux distribution. Obtaining the  $R\theta$ -channel source distribution is simply a matter of integrating the known  $R, \theta, Z$  core source over the axial dimension. (Note that the source will be zero outside of the core region.) Obtaining the weighted cross sections may be more difficult, since the scalar flux appears as a weight function. However, in reactors studied previously, results have not been sensitive to the axial cross section weighting, and the values of the macroscopic cross sections evaluated at  $Z=0$  were found to be adequate.<sup>26</sup>

In summary, the  $R\theta$ -channel flux is obtained by performing an  $R\theta$  transport calculation which uses (1) the axial integrated core source distribution as input for the fixed source and (2) the approximate axially weighted macroscopic cross sections (which in the proposed method can be approximated by the midplane values). Unlike the source for the midplane method,

which is specified per unit height, the R $\theta$ -channel source is equal to the axially integrated value and is thus proportional to the average value, rather than the midplane value. There are no axial leakage terms (i.e., "buckling") in the R $\theta$ -channel transport equation, unlike the midplane equation.

The expression for  $\phi_{RZ}/\phi_R$  appearing in Eq. (4.34) can be viewed as an "axial distribution factor" which distributes the R $\theta$  (axially integrated) solution over the axial dimension. It has been found that, in most cases, this expression can be adequately represented for in-vessel dosimeter calculations by the axial power distribution, i.e.,

$$A(R,Z) \equiv \frac{\phi_{RZ}(R,Z)}{\phi_R(R)} \approx A(Z) \equiv \frac{P(Z)}{\int P(Z)dZ} ,$$

where P(Z) is a single, representative axial power shape. However, for ex-vessel cavity dosimetry analysis, the axial flux distribution in the cavity may be significantly different from the distribution within the vessel. It will be necessary to perform additional transport calculations to obtain  $\phi_{RZ}$  and  $\phi_R$  in these cases. For detectors located beyond the vertical extent of the core, there is evidence that the synthesis method breaks down rather badly in the cavity, but these locations are not important to dosimetry analysis.

The RZ-channel and 1-D R-channel flux equations are obtained in an analogous manner to the R $\theta$  equation. In these cases, the 3-D source is respectively integrated over  $\theta$  to obtain S(R,Z) and over  $\theta$  and Z to obtain S(R). The 2-D RZ and 1-D R transport calculations are then performed to obtain the channel fluxes, and radially-dependant axial distribution functions are obtained by taking the ratio of the RZ and R channel fluxes.

A standard procedure such as one of the two (midplane or single-channel synthesis) methods outlined here, should be adopted for all organizations to use in their RPV analyses.

#### 4.5 CONSOLIDATION OF TRANSPORT CALCULATION AND DOSIMETRY MEASUREMENTS

The previous sections have discussed procedures for performing transport calculations of the RPV fluence and dosimeter activities. In this section, it will be shown how the calculations can be combined with measurements of the surveillance dosimetry to provide the final estimate of the RPV fluence. The recommended approach is to use a least-squares adjustment procedure as discussed in Section 4.5.2. However, until this methodology is adopted, a modified version of the less rigorous "conventional" method can be used. This method is the technique currently employed by many organizations and was described in Section 2. In Section 4.5.1, a modified form of the same basic approach, which is compatible with the adjoint method of computing surveillance dosimeter activities. Also, a crude approach to determining the estimated uncertainty in the calculated results is described.

#### 4.5.1 Adjoint Version of the Conventional Method

In the conventional consolidation method, a constant adjustment factor is applied to all groups of the calculated flux at the surveillance location. Equation (2.10) shows how this factor is usually computed. If the adjoint method discussed in section 4.4.2 is used to account for the time-dependent source variation, then a slightly different expression is needed in order to be consistent with the equation used in calculating the dosimeter activities.

As derived in Eq. (4.24) of the previous section, the computed activity at TOR for dosimeter  $k$  is

$$A_k = \left( \frac{R_k}{R_i} \right) N_{ok} Y_k \sum_j \langle Q_j \psi_i^* \rangle h_j \quad (4.35)$$

where  $\frac{R_k}{R_i}$  = expression in Eq. (4.23) and

$$h_j = e^{-\lambda_k T_j} e^{-\lambda_k (T-t_j)}$$

For multiple cycles, the summation will be over all time steps in all cycles. Assume that the measured activity (corrected to TOR) for this dosimeter is equal to  $\tilde{A}_{meas}^k$ ; then the C/E ratio for dosimeter  $k$  is defined as

$$r_k = \frac{A_k}{\tilde{A}_{meas}^k} \quad (4.36)$$

Note that if the adjoint function in Eq. (4.35) is divided by this factor, then the calculated activity will exactly equal the measured activity. Similar C/E ratios can be obtained for all dosimeters. The average C/E ratio is equal to

$$\bar{r} = \frac{1}{K} \sum_{k=1}^K r_k \quad (4.37)$$

where  $K$  = number of surveillance dosimeters.

The standard deviation in the C/E values is equal to

$$\sigma = \sqrt{\frac{1}{K-1} \sum_{k=1}^K (r_k - \bar{r})^2} \quad (4.38)$$

The standard deviation gives the spread in the C/E values for the different dosimeters about the mean and, thus, is an indication of the consistency between the transport calculations and the measurements. Therefore, this parameter can be used as a crude measure of the uncertainty in the final estimated fluence at the surveillance location.

In order to consolidate the measurements and calculations, simply divide the computed adjoint function by  $r$ , so that the adjoint function is modified to

$$\psi^* \rightarrow \frac{\psi^*}{r} \quad (4.39)$$

When Eq. (4.35) is evaluated with the modified adjoint function, the resulting calculated activities should agree closely with the measured values. It will now be shown how this procedure can be used to obtain a correction to the originally calculated RPV fluence. Let the fluence above 1.0 MeV [indicated as  $\phi(>1)$ ] as the measure of RPV fluence. In order to obtain a better value for  $\phi(>1)$  at the surveillance location, the same scaling procedure is used, and

$$\phi_S(>1) \rightarrow \frac{\bar{\phi}_S(>1)}{\bar{r}} \quad (4.40)$$

Note that the modified adjoint (i.e., divided by  $r$ ) is used in order to take advantage of the measurements; thus, the modification in expression (4.40) represents an adjusted fluence at the surveillance location. The uncertainty in this value is indicated by the standard deviation in the C/E values, assuming that an adequate number of different dosimeters are analyzed.

In order to extrapolate this fluence to the pressure vessel, a lead factor is defined in the usual manner:

$$LF = \frac{\bar{\phi}_S(>1)}{\bar{\phi}_{\max}(>1)} \quad (4.41)$$

where  $\bar{\phi}_{\max}(>1)$  = maximum time-averaged flux at the PV inner radius, as found in the forward calculation.

Recall that, in the approach developed in Section 4.4.2 (unlike most current approaches), the time-averaged fluxes  $\bar{\phi}_S$  and  $\bar{\phi}_{\max}$  correctly reflect the space- and time-dependent distributions in the core source and, thus, should be quite accurate. The adjusted value for the maximum fluence incident on the RPV is then equal to

$$\phi_{RPV}(>1) = \frac{\bar{\phi}_S(>1)}{\bar{r} \cdot LF} \quad (4.42)$$

The uncertainty in the RPV fluence may actually be different than the uncertainty in the surveillance location fluence, due to uncertainties in the lead factor (LF). It is difficult to ascertain the LF uncertainty without performing a detailed sensitivity and uncertainty analysis, such as utilized in some least-squares adjustment codes.<sup>14,27</sup> Unless this rigorous approach is employed, it is necessary to neglect the LF uncertainty and assume that the uncertainty in the RPV fluence is the same as that at the surveillance capsule, which is approximated by the standard deviation in the C/E values, as given by Eq. (4.38).

#### 4.5.2. Least-Squares Consolidation

The current method consolidates the measurements and calculated results through the use of a single adjustment factor which scales the computed fluxes in all groups by a uniform factor [see Eq. (2.10)]. An improved approach is to adjust the group-wise fluxes, which allows changes in both the magnitude and energy distribution of the fluence rate. Several methods with various degrees of sophistication have been developed to perform a consolidation of this type, whereby the measured activities from several different threshold dosimeters are used to "unfold" an adjusted spectrum from the original calculated spectra. All are based on a least-squares approach that modifies the group fluxes in a manner which simultaneously minimizes the overall discrepancy between all the calculated and measured dosimeter activities. The more rigorous methods take into account uncertainties in the calculated group fluxes as well as in the measurements when making the adjustments. Reference 7 describes some of the available least-squares spectral unfolding codes. References 8 and 9 give a detailed description of the least-squares logarithmic adjustment code LSL-M2 and Refs. 14, 27, 28, and 29 present the theory and application of the generalized linear least-squares adjustment code LEPRICON. The FERRET-SAND method has also been used extensively to improve and revise the spectra in LWR surveillance capsules.<sup>30</sup> The latter codes have been extensively applied to RPV fluence determination to obtain adjusted spectra at the surveillance location. The LSL-M2 and LEPRICON methods will be discussed in detail since these provide means for adjusting spectra at more than one location and to extrapolate from surveillance and other dosimetry locations to the interior of the vessel wall.

##### 4.5.2.1. The LSL-M2 Adjustment Procedure

The LSL-M2 program performs the consolidation between calculated spectra and measurements by simultaneously adjusting group fluences, measurements, and dosimetry cross-section data consistent with the relative amount of uncertainty for each data item. All uncertainties must be given in terms of variances and covariances. This is relatively straight-forward for experimental data, and the uncertainties for dosimetry cross sections are available in ENDF or IRDF files which are included in the LSL-M2 package. Determination of variances and covariances for the calculated fluences is much more difficult. The simple scaling, as discussed in Section 4.5.1, assumes perfect correlation between all energy groups at all locations with one overall variance based on C/E values. On the other end of the spectrum is a complete error analysis of the reactor calculation similar to the procedure in the LEPRICON approach. A reasonable compromise is to provide some crude estimates for the variances of the calculated fluences in each energy group and to assign correlations which are large (i.e., correlations coefficient close to 1.0) for neighboring energy groups and neighboring meshpoints within the reactor with gradually diminishing correlations for more distant energies and locations. The calculational tools for such fluence uncertainty estimates are provided in LSL-M2 based on "generic" values obtained from LEPRICON calculations. The reason why such crude estimates may be sufficient is that only variances and covariances for the C/E ratios are used in the adjustment procedure

and these are not too sensitive to changes in fluence variances and covariances. Care should be exercised not to base fluence variances exclusively on C/E ratios. Good C/E ratios may be fortuitous and do not necessarily reflect on the goodness of fluences at energies and locations that are not covered by dosimetry measurements. Somewhat more conservative uncertainty estimates for fluences than those obtained from C/E ratios should be used.

Once all the variances and covariances are determined, LSL-M2 simultaneously adjusts as many spectra as the computer memory allows, e.g., several in-vessel surveillance capsules, cavity measurements plus selected positions inside the vessel wall. Values with uncertainties for the adjusted fluences are provided including damage parameters such as fluence greater than 1.0 MeV or dpa of iron. Inconsistent data are identified for further scrutiny. The LSL-M2 procedure has been used extensively for the metallurgical experiments at the Poolside Facility of the Oak Ridge Research Reactor. Experimental runs with power-reactor data have also been performed. Included in the LSL-M2 package are cross-section files and auxiliary programs to facilitate processing.

#### 4.5.2.2. The LEPRICON Adjustment Procedure

The LEPRICON approach is unique in both the manner in which the adjusted group fluxes are obtained, as well as in its ability to propagate the adjustment from the surveillance location to locations in the RPV. Instead of directly adjusting the calculated flux spectrum, LEPRICON effectively modifies the data used in the transport calculations (e.g., cross sections, fission spectra, bias factors, etc.), which then are responsible for changes to the calculated spectrum. Correlations as well as uncertainties in the calculational and measurement data are considered in the data adjustment (LEPRICON contains an extensive library of covariance data built into the code). First-order sensitivity coefficients stored in the code are used to relate the transport data changes to changes in the group fluxes at the surveillance location. Correlations in the fluxes at the surveillance and RPV locations allow adjustments to be made at the RPV locations as well. As always, the data are modified to minimize the overall discrepancy in a least-squares sense between calculated and measured dosimeter results. In addition to considering the dosimeter measurements of the actual reactor being analyzed, LEPRICON also has a library of dosimeter measurements from many benchmark experiments which are included in the simultaneous least-squares adjustment.

Although the transport data are adjusted to improve the agreement at the surveillance locations, changes in the data used in the transport calculations also affect the computed fluxes in the RPV. This simple fact provides the means for adjusting the flux spectrum within the RPV; as mentioned above, modified transport data are used to obtain an improved estimate for the RPV flux. Theoretically, a new transport calculation could be performed with the modified data, but this would be too expensive. In practice, pre-calculated sensitivity coefficients are used to relate the changes in the transport data to the desired changes in the RPV flux spectrum.

The entire procedure described above is automated in the LEPRICON code. Thus, the measured and calculated dosimeter activities are input to the code, and adjustments in the flux spectra at both the surveillance and RPV locations are output. The LEPRICON approach also has another major side benefit. Because the code contains an extensive library of cross-section uncertainty data (obtained from ENDF/B-V evaluation), it is possible to obtain a realistic estimate of the uncertainty in the original calculated RPV fluence as well as of the adjusted fluence. The adjusted fluence, of course, will have a lower uncertainty than the original fluence. Recent applications of LEPRICON to power reactor analysis have shown that the uncertainty in the estimated RPV fluence is reduced by about a factor of two with this technique. Furthermore, the uncertainty in the results is rigorously computed, so that an actual standard deviation in the fluence can be quantified. This is very important in assessing the reliability of the transport calculations and measurements, and it ensures that safety margins are more realistic.

Therefore, it is recommended that a least-squares adjustment code such as LEPRICON be adopted for consolidating the measured and experimental results.

## 5. CONCLUSIONS AND RECOMMENDATIONS

Little quality assurance requirements or established guidelines are currently available to ensure reliability in the transport calculations done by the various organizations performing RPV fluence analysis. The general methods in use for surveillance dosimetry analysis contain several assumptions and shortcomings which could, at times, compromise the accuracy of the resulting analysis, with no estimates readily available of the uncertainties in or conservatism of the results. Some of these approximations could be especially significant in extended lifetime studies.

This report has outlined specific standardizations and improvements to the present method that could enhance the detail and accuracy in the results with a modest amount of additional effort, using supplementary source data already available from core-follow analysis. Virtually all of the recommendations alluded to have already been incorporated into a series of computer programs written by Oak Ridge National Laboratory under the system name LEPRICON. This software has successfully been applied to the analysis of the Arkansas Nuclear One-Unit 1 and H. B. Robinson-2 reactors.<sup>28,29</sup> As well as to the analysis of over 50 benchmark measurements.<sup>14,26,32,33</sup>

The methods recommended in this analysis can easily accommodate ad hoc dosimetry placed in the reactor cavity as well,<sup>28</sup> which is now becoming more and more commonly used in monitoring RPV fluence reduction measures adopted for plant-life extension. Simultaneous analysis of dosimetry at both a conventional in-vessel location and a cavity location has also been successful.<sup>29</sup>

The need for standardization of data and improved methods having been demonstrated, it is recommended that a Regulatory Guide be written on neutron transport calculations in pressure vessel surveillance dosimetry analysis. It would describe acceptable methods of analysis and recommend the use of specific cross-section libraries and other generalized input to the transport codes. It could also recommend a technique for reconciling discrepancies between calculated and measured dosimeter activities and arriving at defensible uncertainties in the fluences at various RPV locations.

## 6. REFERENCES

1. Code of Federal Regulations, "Domestic Licensing of Production and Utilization Facilities," 10 CFR 50; "General Design Criteria for Nuclear Power Plant," Appendix A; "Fracture Toughness Requirements," Appendix G; "Reactor Vessel Material Surveillance Program Requirements," Appendix H; U.S. Government Printing Office, Washington, DC, current edition.
2. C. Z. Serpan, Jr., "Reliability of Fluence Embrittlement Projections for Pressure Vessel Surveillance Analysis," Nucl. Tech. 12, 108, September 1971.
3. T. U. Marston and K. E. Stalkopf, "Radiation Embrittlement: Significance of Its Effects on Integrity and Operation of LWR Pressure Vessels," Nuclear Safety 21(6), 724, November - December 1980.
4. ASTM Standard E706-81, "Master Matrix for LWR Pressure Vessel Surveillance Standards," 1981 Annual Book of ASTM Standards, American Society for Testing and Materials, Philadelphia, PA, 1981.
5. Regulatory Guide 1.99, "Effects of Residual Elements on Predicted Radiation Damage to Reactor Vessel Materials," Rev. 1, Nuclear Regulatory Commission, Washington, DC, April 1977.
6. W. A. Rhoades and R. L. Childs, An Updated Version of the DOT 4 One- and Two-Dimensional Neutron/Photon Transport Code, ORNL-5851, Oak Ridge National Laboratory, Oak Ridge, TN, July 1982.
7. ASTM E944-83, "Standard Practice for Application of Neutron Spectrum Adjustment Methods in Reactor Surveillance," Annual Book of ASTM Standards, American Society for Testing and Materials, Philadelphia, PA, current edition.
8. F. W. Stallmann, Theory and Practice of General Adjustment and Model Fitting Procedures, NUREG/CR-2222, ORNL/TM-7896, Nuclear Regulatory Commission, Washington, DC, December 1981.
9. F. W. Stallmann, LSL-M2: A Computer Program for Least-Squares Logarithmic Adjustment of Neutron Spectra, NUREG/CR-4349, ORNL/TM-9933, Nuclear Regulatory Commission, Washington, DC, March 1986.
10. G. L. Simmons and R. Roussin, SAILOR - A Coupled Cross Section Library for Light Water Reactors, DLC-76, March 1983.
11. G. L. Simmons and R. W. Roussin, "A New Cross Section Library for LWR Shielding and Pressure Vessel Dosimetry Applications," Proc. of the Conference on 1980 Advances in Reactor Physics and Shielding, Sun Valley, CA, September 14-19, 1980, American Nuclear Society, Hinsdale, IL, 1980.

12. C. Y. Fu and D. M. Hetrick, "Evaluation and Testing of Double Differential Fe(n,n') Cross Sections," Trans. Am. Nucl. Soc., Washington, DC, November 16-20, 1986.
13. C. Y. Fu and D. M. Hetrick, "Experience in Using the Covariances of Some ENDF/B-V Dosimeter Cross Sections: Proposed Improvements and Addition of Cross-Reaction Covariances," Proc. of the 4th ASTM-EURATOM Symposium on Reactor Dosimetry, Gaithersburg, MD, March 22-26, 1982, NUREG/CP-0029, Nuclear Regulatory Commission, Washington, DC, Vols. 1 and 2, July 1982.
14. R. E. Maerker, J. J. Wagschal, and B. L. Broadhead, Development and Demonstration of an Advanced Methodology for LWR Dosimetry Applications, EPRI NP-2188, Electric Power Research Institute, Palo Alto, CA, December 1981.
15. M. L. Williams, M. Landesman, and F. B. K. Kim, Calculation of the Power Distribution in the VENUS PWR Mock-Up Benchmark Using Two-Group Diffusion Theory, NUREG/CR-4647, ORNL/TM-10095, Nuclear Regulatory Commission, Washington, DC, August 1986.
16. W. R. Cadwell, PDQ-7 Reference Manual, WAPD-TM-673, Westinghouse Electric Corporation, Bettis Atomic Power Laboratory, January 1967.
17. A. Ahlin and M. Edenius, "CASMO - A Fast Transport Theory Assembly Depletion Code for LWR Analysis," Trans. Am. Nucl. Soc. 26, 604, 1977.
18. M. L. Williams, DOTSOR: A Module in the LEPRICON Computer Code System for Representing the Neutron Source Distribution in LWR Cores, EPRI Report (to be published).
19. R. E. Maerker, B. L. Broadhead, and M. L. Williams, "Recent Progress and Developments in LWR-PV Computational Methodology," Proc. of the 5th ASTM-EURATOM Symposium on Reactor Dosimetry, Geesthacht, Federal Republic of Germany, September 24-28, 1984, EUR 9869, Commission of the European Communities, 1985.
20. R. E. Maerker, M. L. Williams, and B. L. Broadhead, "Accounting for Changing Source Distributions in Light Water Reactor Surveillance Dosimetry Analysis," Nucl. Sci. Eng. 94, 291, 1986.
21. G. C. Martin, Browns Ferry Unit 3 In-Vessel Neutron Spectral Analysis, NEDO-24793, General Electric Company, San Jose, CA, August 1980.
22. G. I. Bell and S. Glasstone, Nuclear Reactor Theory, Van Nostrand Reinhold Co., New York, 1970.
23. R. E. Maerker, M. L. Williams, and B. L. Broadhead, TIMEPATCH: A Module in the LEPRICON Computer Code System for Evaluating Effects of Time-Dependent Source Distributions in PWR Surveillance Dosimetry, EPRI Report (to be published).

24. H. B. Robinson Fluence Reduction Analysis for the Partial-Length Shield Assembly Concept, TEC Report R-83-030, Technology for Energy Corporation and Carolina Power and Light Company, 1983.
25. M. L. Williams, P. Chowdhury, and B. L. Broadhead, DOTSYN: A Module in the LEPRICON Computer Code System for Synthesizing Three-Dimensional Fluxes, EPRI Report (to be published).
26. R. E. Maerker and B. A. Worley, Activity and Fluence Calculations for Startup and Two-Year Irradiation Experiments Performed at the Poolside Facility, NUREG/CR-3886, ORNL/TM-9265, Nuclear Regulatory Commission, Washington, DC, October 1984.
27. R. E. Maerker, B. L. Broadhead, and J. J. Wagschal, "Theory of a New Unfolding Procedure in PWR Pressure Vessel Dosimetry and Development of an Associated Benchmark Database," Nucl. Sci. Eng. 91, 369, 1985.
28. R. E. Maerker et al., "Application of the LEPRICON Unfolding Procedure to the Arkansas Nuclear One-Unit 1 Reactor," Nucl. Sci. Eng. 93, 137, 1986.
29. R. E. Maerker, LEPRICON Analysis of Pressure Vessel Surveillance Dosimetry Inserted into H.B. Robinson-2 During Cycle 9, NUREG/CR-4439, ORNL/TM-10132, Nuclear Regulatory Commission, Washington, DC, August 1986; also Nucl. Sci. Eng. 96, 263, 1987.
30. W. N. McElroy, ed., LWR Pressure Vessel Surveillance Dosimetry Improvement Program, NUREG/CR-3319, HEDL-TME 85-3, Nuclear Regulatory Commission, Washington, DC, August 1985.
31. M. L. Williams et al., The ELXSIR Cross-Section Library for LWR Pressure Vessel Irradiation Studies: Part of the LEPRICON Computer Code System, EPRI NP-3654, Electric Power Research Institute, Palo Alto, CA, September 1984.
32. R. E. Maerker et al., Revision and Expansion of the Data Base in the LEPRICON Dosimetry Methodology, EPRI NP-3841, Electric Power Research Institute, Palo Alto, CA, January 1985.
33. R. E. Maerker, Analysis of the NESDIP2 and NESDIP3 Radial Shield and Cavity Experiments, NUREG/CR-4886, ORNL/TM-10389, Nuclear Regulatory Commission, Washington, DC, May 1987.

NUREG/CR-5049  
 ORNL/TM-10651  
 Dist. Category R5

#### INTERNAL DISTRIBUTION

- |                       |                                      |
|-----------------------|--------------------------------------|
| 1. C. A. Baldwin      | 15. L. F. Miller                     |
| 2. W. G. Craddick     | 16. R. K. Nanstad                    |
| 3. W. R. Corwin       | 17. C. E. Pugh                       |
| 4-9. F. B. K. Kam     | 18. F. W. Stallmann                  |
| 10. A. L. Lotts       | 19. Document Reference Section       |
| 11. R. E. Maerker     | 20. Central Research Library         |
| 12. J. R. Merriman    | 21-22. Laboratory Records Department |
| 13. A. P. Malinauskas | 23. Laboratory Records - ORNL R.C.   |
| 14. F. R. Mynatt      | 24. ORNL Patent Office               |

#### EXTERNAL DISTRIBUTION

25. John Carew, Brookhaven National Laboratory Upton, Department of Nuclear Energy, Bldg. 130, Long Island NY 11973
26. A. Fabry, CEN/SCK, Reactor Physics Department, Boeretang 200, B-2400 Mol, Belgium
27. Lambros Lois, U.S. Nuclear Regulatory Commission, Phillips Building, Mail Stop P-924, Washington DC 20555
28. M. E. Mayfield, Division of Engineering Technology, U.S. Nuclear Regulatory Commission, Washington DC 20555
29. W. N. McElroy, Hanford Engineering Development Laboratory, P.O. Box 1970, Mail Stop W/C-39, Richland WA 99352
30. E. D. McGarry, National Bureau of Standards, Center for Radiation Research, Bldg. 235, Room 2155, Gaithersburg MD 20899
31. C. Z. Serpan, Division of Engineering Technology, U.S. Nuclear Regulatory Commission, Mail Stop SS-1130, Washington DC 20555
32. A. Taboada, Division of Engineering Technology, U.S. Nuclear Regulatory Commission, Mail Code NL 5650, Washington DC 20555
33. M. L. Williams, Nuclear Science Center, Louisiana State University, Baton Rouge LA 70803-5820
34. Assistant Manager for Energy Research and Development, U.S. Department of Energy, Oak Ridge Operations Office, Oak Ridge TN 37830
- 35-36. Technical Information Center, U.S. Department of Energy, Oak Ridge TN 37830
- 37-351. Given distribution under category R5 (10 copies - NTIS)

NRC FORM 325 (2-84) NRCM 1102 3201, 3202	U.S. NUCLEAR REGULATORY COMMISSION	1 REPORT NUMBER (Assigned by T/D, add Vol. No., if any)				
<b>BIBLIOGRAPHIC DATA SHEET</b>		NUREG/CR-5049 ORNL/TM-10651				
SEE INSTRUCTIONS ON THE REVERSE		3 LEAVE BLANK				
2 TITLE AND SUBTITLE  Pressure Vessel Fluence Analysis and Neutron Dosimetry		4 DATE REPORT COMPLETED				
5 AUTHOR(S)  F. B. K. Kam, R. E. Maerker, M. L. Williams, and F. W. Stallmann		<table border="1" style="width: 100%;"> <tr> <td style="width: 50%;">MONTH</td> <td style="width: 50%;">YEAR</td> </tr> <tr> <td style="text-align: center;">November</td> <td style="text-align: center;">1987</td> </tr> </table>	MONTH	YEAR	November	1987
MONTH	YEAR					
November	1987					
7 PERFORMING ORGANIZATION NAME AND MAILING ADDRESS (Include Zip Code)		<table border="1" style="width: 100%;"> <tr> <td style="width: 50%;">MONTH</td> <td style="width: 50%;">YEAR</td> </tr> <tr> <td></td> <td></td> </tr> </table>	MONTH	YEAR		
MONTH	YEAR					
Oak Ridge National Laboratory P.O. Box X Oak Ridge, Tennessee 37831		8 PROJECT/TASK/WORK UNIT NUMBER				
10 SPONSORING ORGANIZATION NAME AND MAILING ADDRESS (Include Zip Code)		9 FIN OR GRANT NUMBER				
Division of Engineering Office of Nuclear Regulatory Research U.S. Nuclear Regulatory Commission Washington, D.C. 20555		B0415				
12 SUPPLEMENTARY NOTES		11 TYPE OF REPORT				
13 ABSTRACT (200 words or less)		Topical				
<p>A review of the various methodologies used by industries and research institutes for reactor pressure vessel (RPV) fluence determination shows that most organizations employ an analysis sequence consisting of three steps. These include transport calculations, dosimetry measurements, and a statistical procedure to combine the calculations and measurements to arrive at a fluence value which has a smaller uncertainty than the original calculations. An accurate determination of damage fluence accumulated by the RPV as a function of space and time is essential in order to ensure the vessel integrity for both pressurized thermal shock transients and end-of-life considerations. The desired accuracy for neutron exposure parameters such as displacements per atom or neutron fluence (<math>E &gt; 1.0</math> MeV) is on the order of <math>\pm 10\%</math> to <math>\pm 15\%</math> (<math>1\sigma</math>). These types of accuracies can only be obtained realistically by validation of the entire analysis sequence in benchmark experiments. This report identifies a standardized procedure based on benchmarked calculations, data, and dosimetry measurements, which could be used by organizations performing RPV fluence determinations. Another purpose of this report is to provide supporting documentation for any proposed regulatory guide on this subject.</p>		6 PERIOD COVERED (Inclusive Dates)				
14 DOCUMENT ANALYSIS - KEYWORDS/DESCRIPTORS	15 AVAILABILITY STATEMENT					
5 IDENTIFIERS/OPEN-ENDED TERMS	Unlimited					
	16 SECURITY CLASSIFICATION					
	<i>(This page)</i> Unclassified					
	<i>(This report)</i> Unclassified					
	17 NUMBER OF PAGES					
	18 PRICE					

120555078877 1 1AN1R5  
US NRC-OARM-ADM  
OFF OF PUB SVCS  
POLICY & PUB MGT BR-PDR NURZG  
W-537  
WASHINGTON DC 20555